CIS is a potent checkpoint in NK cell-mediated tumor immunity

Rebecca B. Delconte*[1,2], Tatiana B. Kolesnik*[1], Laura F. Dagley*[1,2], Jai Rautela[1,2], Wei Shi[1,2], Eva M. Putz[3,], Kimberly Stannard[3], Jian-Guo Zhang[1,2], Charis Teh[1,2], Matt Firth[1,2], Takashi Ushiki[1,2], Christopher E. Andoniou[4], Mariapia A. Degli-Esposti[4] , Phillip P. Sharp[1,2], Caroline E. Sanvitale[5], Giuseppe Infusini[1], Nicholas P.D Liau[1,2], Edmond M. Linossi[1,2], Christopher J. Burns[1,2], Sebastian Carotta[1,2], Daniel H.D. Gray[1,2] Cyril Seillet[1,2], Dana S. Hutchinson[6], Gabrielle T. Belz[1,2], Andrew I. Webb[1,2], Warren S. Alexander[1,2], Shawn S. Li[7], Alex N. Bullock[5], Jeffery J. Babon[1,2], Mark J. Smyth[3,8], Sandra E. Nicholson[#1,2] and Nicholas D. Huntington[#1,2]

[1]The Walter and Eliza Hall Institute of Medical Research, Parkville, Victoria 3050, Australia;
[2]Department of Medical Biology, The University of Melbourne, VIC 3010, Australia;
[3]Immunology in Cancer and Infection Laboratory QIMR Berghofer Medical Research Institute, Herston, QLD 4006, Australia.
[4]Immunology and Virology Program, Centre for Ophthalmology and Visual Science, The University of Western Australia and Centre for Experimental Immunology, Lions Eye Institute, Nedlands, Western Australia, Australia.
[5]Structural Genomics Consortium (SGC), University of Oxford, Old Road Campus, Roosevelt Drive, Oxford OX3 7DQ, UK.
[6]Monash Institute of Pharmaceutical Sciences, Monash University, Parkville, VIC 3052, Australia.
[7]Department of Biochemistry and the Siebens-Drake Medical Research Institute, Schulich School of Medicine and Dentistry, University of Western Ontario, London, ON N6A 5C1, Canada.
[8]School of Medicine, University of Queensland, Herston, QLD 4006, Australia.

* These authors contributed equally to this work
\# These authors jointly directed this work

Key words: cancer, immunotherapy, checkpoint, IL-15, NK cell, CIS, JAK1, JAK3, metastases

Corresponding authors:

Dr Nicholas D Huntington
Immunology Division
Email: huntington@wehi.edu.au

Dr Sandra E. Nicholson
Inflammation Division
Email: snicholson@wehi.edu.au

The Walter and Eliza Hall Institute
1G Royal Pde, Parkville,
Victoria, 3052, Australia
Phone: +613 9345 2555

Abstract (150 words)

The detection of aberrant cells by natural killer (NK) cells is controlled by the integration of signals from activating and inhibitory ligands and from cytokines such as IL-15. Here we have identified CIS (encoded by *Cish*) as the critical negative regulator of IL-15 signaling in NK cells. *Cish* was rapidly induced in response to IL-15 and deletion of *Cish* rendered NK cells hypersensitive to IL-15, as evidenced by enhanced proliferation, survival, IFN-γ production and cytotoxicity towards tumors. This was associated with increased JAK-STAT signaling in NK cells in which *Cish* was deleted. Correspondingly, CIS interacted with the tyrosine kinase JAK1, inhibiting its enzymatic activity and targeting JAK for proteasomal degradation. *Cish*$^{-/-}$ mice were resistant to melanoma, prostate and breast cancer metastasis *in vivo*, and this was intrinsic to NK cell activity. This study has uncovered a potent intracellular checkpoint in NK cell-mediated tumor immunity and holds promise for novel cancer immunotherapies directed at blocking CIS function.

Introduction

The immune system has a key role in controlling tumor growth and metastasis. Cytotoxic lymphocytes such as natural killer (NK) and $CD8^+$ effector T cells contribute to anti-tumor immunity through cancer immunoediting[2]. Normal $CD8^+$ effector T cell function is controlled by the expression of regulatory proteins. The identification and therapeutic inhibition of these so-called "checkpoints" has dramatically improved cancer outcomes, especially in metastatic melanoma. In particular, antibodies that block the $CD8^+$ T cell inhibitory receptor, PD-1 from interacting with its ligand effectively enhance the $CD8^+$ T cell anti-tumor immune response[5]. Although T cell checkpoint inhibitors have revolutionized cancer immunotherapy, their effectiveness appears limited to patients with tumor infiltrating $CD8^+$ T cells and while many of these patients present durable responses, some tumors develop resistance to checkpoint inhibition[6].

NK cells are also of interest as immunotherapeutic targets[7]. They are bone marrow-derived innate lymphocytes that frequent blood and lymphoid tissues and possess spontaneous anti-tumor activities[8]. NK cells can eliminate tumors directly, and this activity is governed by the integration of signals from activating and inhibitory ligands and from cytokines such as IL-12, IL-18 and IL-15. Inhibitory receptors engage molecules present on healthy host cells including MHC-I, cadherins and glycoproteins. Conversely, activating receptors engage with host-encoded ligands that are induced as a result of viral infection or DNA damage (induced self-recognition)[7,8].

The pleiotropic cytokine IL-15 is an important regulator of NK cell development, homeostasis and activation[9]. Membrane-bound IL-15-IL-15 receptor alpha (IL-15Rα) complex is trans-presented by a neighboring cell to a heterodimer consisting of the IL-2R β and γ_c subunits (CD122/CD132) on the surface of NK cells. IL-15 binding then induces activation of the β/γ_c-associated JAK1 and JAK3 tyrosine kinases, recruitment and activation of STAT5, and transcription of STAT5-target genes, which drive survival, proliferation and encode cytotoxic agents such as granzymes[9-12]. Systemic delivery of IL-15 has been trialed as a cancer therapy, however enthusiasm for its use has been tempered by toxicity[13]. Thus novel approaches that deliver IL-15 more precisely to the target cell or specifically render the target cell more responsive to IL-15 are appealing avenues for investigation.

Despite this, we still do not understand how intracellular IL-15 signaling is switched off. The suppressor of cytokine signaling (SOCS) proteins (CIS, SOCS1-7)[14] are intracellular negative regulators often induced to limit cytokine signaling in a classic negative feedback loop[15]. They are characterized by a central SH2 domain, which binds to phosphorylated tyrosine motifs in target proteins and a C-terminal SOCS box sequence motif. The SOCS box enables the SOCS proteins to function as adaptors for an E3 ubiquitin ligase complex that ubiquitinates SOCS-interacting proteins, directing them to proteasomal degradation[16]. In addition to recruitment of the E3 ligase

complex, SOCS1 and SOCS3 bind directly to JAK1, JAK2 and TYK2, inhibiting JAK enzymatic activity[17,18]. *Cish* induction was first demonstrated in response to IL-3, IL-2 and erythropoietin and exogenous expression of CIS inhibited signaling through these receptors[19-21]. Consistent with its induction by IL-2 family cytokines, *Cish* deletion augmented IL-4 and IL-2 signaling in $CD4^+$ T cells[22]. Somewhat surprisingly, it was also shown to regulate antigen receptor signaling in $CD8^+$ T cells[23]. Although it was the first SOCS protein to be discovered, relatively little is known about physiological CIS target proteins and its mechanism of inhibition.

Here we identify CIS as a key suppressor of IL-15 signaling in NK cells. $Cish^{-/-}$ NK cells are hypersensitive to IL-15 and as a result, $Cish^{-/-}$ mice are resistant to experimental tumor metastasis. Loss of CIS resulted in heightened and prolonged IL-15-driven JAK-STAT signaling in NK cells and we identified JAK1 as a novel target for direct inhibition by CIS. CIS is therefore an important intracellular checkpoint in NK cell-mediated tumor immunity, and we suggest that blockade of the CIS:JAK1 interaction may form the basis of new cancer immunotherapies.

RESULTS

Phenotype of CIS-deficient NK cells

To investigate IL-15 signaling, we profiled IL-15-induced SOCS expression in NK cells. *Cish*, *Socs1*, *Socs2* and *Socs3* mRNA were induced in NK cells within 2 h of IL-15 treatment, with the early and transient induction of *Cish* typifying *Socs* induction by its target cytokine (**Fig. 1a**). Consistent with the rapid induction of mRNA in saturating concentrations of IL-15, CIS protein was detected in NK cell lysates within 1 h of stimulation (**Fig. 1b**). In addition to the induction of *Cish* by IL-15, *Cish* was expressed throughout NK cell development, with the highest expression observed early in NK cell differentiation (NK cell progenitors and immature bone marrow-derived NK cells; **Supplementary Fig. 1a**).

To investigate the physiological role of CIS in IL-15 signaling, we utilized a germline *Cish*-deleted mouse ($Cish^{-/-}$)[23], first confirming that *Cish* mRNA and protein were absent from NK cells (**Supplementary Fig. 1b**). *Cish*-null mice were healthy, fertile and did not present with any phenotypic abnormality. Lymphocyte frequencies, including conventional NK cells, liver-resident type 1 innate lymphoid cells (ILC1) and lung-resident ILC2, were normal in $Cish^{-/-}$ mice (**Fig. 1c**, **Supplementary Fig. 1c-g**). Similarly, NK cell expression of the activating receptors NK1.1 and NKp46 was normal (**Fig. 1d**) as was the development and response of conventional $CD4^+$ and $CD8^+$ T cells[23] and regulatory T cells in the absence of *Cish* (**Supplementary Fig. 2a-c**). When either irradiated wild-type mice reconstituted 50:50 with $Cish^{+/+}$:$Cish^{-/-}$ bone marrow, or $Cish^{-/-}$ mice were infected with murine cytomegalovirus (MCMV), we detected normal expansion and

contraction of Ly49H^{+} NK cells and comparable numbers of MCMV-specific CD8^{+} T cells in *Cish*$^{+/+}$ and *Cish*$^{-/-}$ mice (**Supplementary Fig. 2d-e**).

NK cell development was also normal in *Socs1*$^{-/-}$ and *Socs3*$^{-/-}$ single or doubly-deficient mice (**Supplementary Fig. 3a**). However, in contrast to *Socs1*$^{-/-}$ or *Socs1*$^{-/-}$*Socs3*$^{-/-}$ NK cells, *Cish*$^{-/-}$NK cells displayed a profound hyper-proliferation in response to IL-15 *in vitro* (**Fig. 1e, Supplementary Fig. 3b**). When *Cish*$^{-/-}$ and *Cish*$^{+/+}$ NK cells were co-cultured 1:1 in a titration of IL-15, *Cish*$^{-/-}$ NK cells demonstrated enhanced proliferation at concentrations greater than 5 ng/ml (**Fig. 1e**). Furthermore, *Cish*$^{-/-}$ NK cells represented ~95% of cells recovered from co-culture in non-mitogenic IL-15 concentrations, thus demonstrating superior IL-15-mediated NK cell survival in the absence of CIS (**Fig. 1e**). The hyper-sensitivity of *Cish*$^{-/-}$ NK cells also manifested in an enhanced IL-15-driven IFN-γ production, that was further heightened with co-stimulation via the activating receptors NKp46 and NK1.1, suggesting an important role for IL-15 in synergizing with these receptors (**Fig. 1f**). When co-cultured with Chinese hamster ovarian (CHO) target cells, *Cish*$^{-/-}$ NK cells displayed greater cytotoxicity at low ratios of NK:target cells when compared to *Cish*$^{+/+}$ NK cells (**Fig. 1g and Supplementary Fig. 3c**). *Cish*$^{-/-}$ NK cells also killed B16F10 melanoma cells more efficiently than *Cish*$^{+/+}$ NK cells and produced increased levels of intracellular granzymes when challenged with RMA-m157 cells, evidence that NK cells are broadly hyper-cytotoxic in the absence of *Cish* (**Supplementary Fig. 3c, d**).

To examine the extent of aberrant IL-15 signaling in *Cish*-null NK cells, we performed 100 bp single-ended RNA sequencing on *Cish*$^{+/+}$ and *Cish*$^{-/-}$ NK cells, either purified directly from the spleen (*ex vivo*) or following cultivation in IL-15 (*in vitro*). Very few differentially expressed genes were observed in *ex vivo Cish*$^{-/-}$ NK cells (**Supplementary Fig. 4a**) and this, coupled with the normal frequency of *Cish*$^{-/-}$ NK cells *in vivo* and low expression of *Cish* in mature NK cells, suggests that CIS is not a major regulator of NK cell biology in the steady-state. In contrast, more than 1000 differentially expressed genes were detected in *Cish*$^{-/-}$ NK cells exposed to high concentrations of IL-15 *in vitro* (**Fig. 2 and Supplementary Fig. 4**). The highest up-regulated genes included members of the killer cell lectin-like receptor *Klra1* and *Klra6* and those associated with NK cell effector functions such as the serine proteases *Gzme, Gzmf, Gzmd, Gzmg* and their inhibitors *Serpinb9b, Serpinb9* and *Serpin1a* (**Fig. 2 and Supplementary Fig. 4a**). These findings identify a unique and non-redundant role for CIS as a key negative regulator of IL-15-mediated NK cell effector function. Further, they suggest that CIS acts as an immune checkpoint controlling NK cell responses.

CIS targets the JAK-STAT pathway

Cish$^{-/-}$ splenic NK cells displayed a modest increase in CD122 expression when compared to *Cish*$^{+/+}$ cells, and this difference was heightened following short-term culture in IL-15 (**Fig. 3a**). We next investigated whether the change in receptor levels impacted on IL-15 signaling. The magnitude of IL-15-stimulated JAK1 tyrosine phosphorylation was increased in both freshly isolated and cultured *Cish*$^{-/-}$ NK cells in comparison to control cells, and was coupled with extended phosphorylation kinetics (**Fig. 3b-d**). Interestingly, total JAK1 was elevated in *Cish*$^{-/-}$ NK cells and this was evident in resting cells prior to stimulation (**Fig. 3b,c**). The higher JAK1 and IL-2Rβ levels in freshly isolated *Cish*$^{-/-}$ NK cells (**Fig. 3b**) may result from exposure to low concentrations of IL-15 *in vivo*. CIS itself is most likely cleared during the time taken to isolate primary NK cells. Similarly, in cells expanded in IL-15, we observed higher basal expression of JAK1 after withdrawal of cytokine (**Fig. 3c**). Increased JAK phosphorylation correlated with increased phosphorylation of its substrate, STAT5. In contrast, the absence of *Cish* had no effect on IL-15-dependent AKT phosphorylation (**Fig. 3b-d**), suggesting a unique disconnect between IL-15-driven JAK-STAT and PI3K-mTOR-AKT pathways. This was further confirmed by normal mitochondrial respiration and glycolysis, cellular outcomes that are regulated by AKT activity (**Supplementary Fig. 5a**).

A mass spectrometry-based approach quantifying changes in active JAK levels was used to confirm the elevated JAK1 activity and examine the selectivity of the CIS-deficient effects. A pan-JAK inhibitor (derived from CYT-387; JAK1/2/3) was synthesized, coupled to Sepharose beads and used as an affinity-capture reagent, prior to tryptic digest and mass spectrometric analysis. As the inhibitor binds to the ATP binding site in the kinase domain[24], kinases in the active conformation are preferentially enriched. JAK1 and JAK3 peptides were detected in NK cell lysates with increased number and intensity in *Cish*$^{-/-}$ cells (**Fig. 4a**). CYT-387 has known off-target binding to other kinases, notably TBK1 and CDK2[24], enabling us to perform a restricted kinome analysis on *in vitro* derived *Cish*$^{+/+}$ and *Cish*$^{-/-}$ NK cells (**Supplementary Fig. 5b**). Sixty-nine kinases were enriched relative to their abundance in cell lysates, with 16 kinases differentially regulated in *Cish*$^{-/-}$ cells. The increased activity was largely attributed to kinases involved in regulating cellular proliferation (for example CDK1/2, Prkr, Aurora kinases) (**Fig. 4b, c and Supplementary Data Table 1**). These data are consistent with the hyper-proliferative phenotype and suggest that much of the increased kinase activity is secondary to the increase in IL-15 signaling. A label-free global proteomic analysis also highlighted changes reflecting the enhanced proliferative capacity (cell cycle, DNA replication, cytoskeletal reorganization; **Supplementary Fig. 5c, d and Supplementary Data Table 2**). Taken together, these data highlight a critical role for CIS in inhibiting IL-15-dependent kinase activity in NK cells.

CIS binds to the JAK activation loop

Like other SOCS proteins, CIS contains an SH2 domain, which binds to phosphorylated tyrosine motifs in target proteins and a SOCS box, which together with Elongins B and C, the scaffold protein Cullin5 and the RING protein Rbx2, constitutes an E3 ubiquitin ligase. Given that the increased levels of total JAK1 and 3 protein observed in *Cish*$^{-/-}$ NK cells were not due to increased RNA levels (**Supplementary Fig. 6a**), we investigated the possibility that CIS might directly reduce JAK protein expression through ubiquitination and proteasomal degradation. Previously, CIS had been shown to interact with the IL-2Rβ and was proposed to regulate signaling by blocking recruitment of STAT proteins to the receptor complex[20,21]; however, there is limited evidence to support the latter proposition. As a preliminary step towards identifying CIS target proteins, we performed a screen using a recombinant trimeric complex composed of a human GST-CIS construct (hCIS-SH2; residues 66-258) coupled to GST and Elongins B and C (hCIS-SH2-BC) against a panel of phosphotyrosine peptides corresponding to tyrosines within the IL-2 receptor complex (**data not shown**). Isothermal calorimetry (ITC) was then used to validate binding to phosphopeptides identified in the screen. The hCIS-SH2-BC complex bound with high affinity (0.8-2.1 μM) to synthetic phosphorylated peptides corresponding to tyrosines within the IL-2Rβ cytoplasmic domain (Tyr355, Tyr361 and Tyr392), and within the JAK1 and JAK3 activation loops (Tyr1034 and Tyr980, respectively) (**Table 1; Supplementary Fig. 6b, c**).

We next investigated whether CIS could regulate JAK levels in the absence of the IL-2 receptor complex. Over-expression of JAK in 293T cells (which lack the IL-2R) results in constitutive JAK autophosphorylation. Co-expression of CIS or SOCS1 reduced JAK1 levels to a comparable extent, with a corresponding decrease in JAK1 phosphorylation. In contrast, SOCS3 was unable to inhibit JAK activity in this assay (SOCS3 requires receptor binding) (**Fig. 5a**). Surprisingly, although we observed CIS binding to the JAK3 Tyr980 peptide (**Table 1**), JAK3 phosphorylation was not inhibited in this assay (**Fig. 5a**). We then investigated which CIS domains were required for JAK1 inhibition. Mutation of either the CIS-SH2 domain (R107K) or the Cullin-5 binding site in the SOCS box (P241A/L242A/P243A) was sufficient to diminish CIS inhibitory activity (**Fig. 5b**). Further, pre-incubation of the cells with a proteasomal inhibitor (MG132) reduced CIS-mediated regulation of JAK1 phosphorylation (**Fig. 5b**), supporting a model whereby CIS binds to JAK1 via its SH2 domain and then targets JAK1 for proteasomal degradation. Co-immunoprecipitation was used to demonstrate complex formation between JAK1 and CIS (**Fig. 5c**). To formally demonstrate CIS-mediated ubiquitination of JAK1, Flag-tagged full-length JAK1 protein (generated by expression in 293T cells) was incubated in a cell-free system with recombinant hCIS-SH2-BC complex, Cullin5, Rbx2, E1, E2 (UbcH5c) and free ubiquitin. CIS effectively mediated ubiquitination of phosphorylated JAK1 as indicated by the high molecular

weight species detected by immunoblot analysis (**Fig. 5d**). Together, these data demonstrate that CIS is capable of directly regulating JAK protein expression.

Previously, only SOCS1 and SOCS3 have been shown to bind to and regulate JAK activity. SOCS1 and SOCS3 inhibit JAK via non-canonical SH2 binding to a "GQM" motif present in the JAK1, JAK2 and TYK2 insertion loops and binding of the kinase inhibitory region (KIR) to the catalytic cleft[18]. CIS does not contain a "KIR" region and there was no prior suggestion that it was able to regulate JAK enzymatic activity. However, evidence suggested that an additional mechanism was involved. Firstly, we occasionally observed inhibition of JAK1 phosphorylation in the absence of changes in total JAK1 levels (**Fig. 5b**). Secondly, despite MG132 treatment of wild-type NK cells resulting in an increase in phosphorylation of endogenous JAK1, we did not observe extended kinetics and indeed, JAK phosphorylation was rapidly curtailed. This correlated with increased expression of CIS, which was protected from proteasomal degradation (**Fig. 6a**). We therefore asked whether CIS could inhibit JAK1 kinase activity. Using an *in vitro* kinase assay, the CIS-SH2-BC complex was able to inhibit JAK1 phosphorylation of a substrate peptide with an IC_{50} of 0.12 ± 0.02 μM. CIS inhibition of JAK1 was 20-fold or greater than its inhibition of JAK2 (2.4 ± 1.4 μM), JAK3 (6.7 ± 3.5 μM) or TYK2 (>20 μM) (**Fig. 6b**), suggesting a unique interface with JAK1 in addition to a canonical SH2 interaction with the conserved JAK activation-loop tyrosine. This concept was supported by the only partial reduction of inhibition seen when the JAK1 activation loop peptide was used as a competitor (**Supplementary Fig. 6d**). Although CIS displayed specificity towards JAK1, it inhibited with ~100-fold lower efficiency that SOCS1 (**Fig. 6c**). This suggests that the absolute level of CIS versus SOCS1 will contribute to both specificity and dominance. In this context, receptor recruitment of CIS may increase local concentration of CIS, enabling it to efficiently inhibit JAK1 activity (**Supplementary Fig. 6e**). The post-translational regulation of CIS levels, be it proteasome or protease, adds another exquisite layer of control. These data suggest a new target (JAK1) and mechanism (kinase inhibition) for CIS action, and raise the possibility that CIS is fundamentally more similar to SOCS1 than previously thought.

Cish$^{-/-}$ NK cells protect against experimental metastasis

Inflammation associated with tumor formation is likely to increase IL-15 trans-presentation by stroma or infiltrating myeloid lineages and augment resident NK cell activity[25]. We investigated whether IL-15-induction of CIS acts as a checkpoint in NK cells *in vivo*, challenging *Cish*$^{+/+}$ and *Cish*$^{-/-}$ mice with a panel of syngeneic tumor cell lines, known to activate and be controlled by NK cells. Intravenous (i.v.) administration of B16F10 melanoma cells to *Cish*$^{+/+}$ mice resulted in extensive metastatic nodule formation in the lungs by 14 days. In contrast, B16F10 metastatic nodules were largely absent from *Cish*$^{-/-}$ mice (**Fig. 7a** and **Supplementary Fig. 7a)**. Injection of

Cish$^{+/+}$ and *Cish*$^{-/-}$ mice with a melanoma cell line expressing a mutated form of the serine-threonine kinase *braf* (LWT1 BRAF^{V600E})[26], also resulted in significantly reduced lung metastases in CIS-deficient mice (**Fig. 7b**). This finding was not limited to melanoma, as similar differences in lung metastasis were observed when using the RM-1 prostate cancer cell line (**Fig. 7c**). To confirm that the reduced B16F10 metastasis observed in *Cish*$^{-/-}$ mice was dependent on enhanced NK cell activity, *Cish*$^{+/+}$ and *Cish*$^{-/-}$ mice were treated with anti-asiolo GM1 (to deplete NK cells), anti-CD8 (to deplete CD8^{+} T cells), anti-IFN-γ (to block IFN-γ activity) or control immunoglobulin (cIg). Depletion of NK cells or neutralization of IFN-γ, but not depletion of CD8^{+} T cells, rendered *Cish*$^{-/-}$ mice susceptible to B16F10 metastasis (**Fig. 7d**), identifying a role for CIS in the negative regulation of NK cell activity and IFN-γ in this model. Furthermore, in an NK cell adoptive transfer model using NK cell-null mice as recipients (*Mcl1*$^{f/f}$ *Ncr1-iCre; Ncr1*$^{Mcl1\,\Delta/\Delta}$), *Ncr1*$^{Mcl1\,\Delta/\Delta}$ mice that received *Cish*$^{-/-}$ NK cells had significantly fewer B16F10 lung metastases than mice receiving *Cish*$^{+/+}$ NK cells (**Fig. 7e** and **Supplementary Fig. 7b**), evidence that *Cish*$^{-/-}$ NK cells are intrinsically more active.

Combination immunotherapy using antibodies against PD-1 and CTLA-4 is currently one of the most effective treatments against advanced melanoma[27,28]. To compare this benchmark immunotherapy with *Cish* deletion, *Cish*$^{+/+}$ and *Cish*$^{-/-}$ mice were injected with a high dose of B16F10 melanoma (to elicit both an NK cell and CD8^{+} T cell response) and treated with a combination of anti-PD-1 and anti-CTLA-4 or cIg. Anti-PD-1 and anti-CTLA-4 treatment significantly reduced melanoma metastases when compared to cIg in *Cish*$^{+/+}$ mice, however this was inferior to the protection afforded by *Cish*-deletion alone (*Cish*$^{-/-}$ mice + cIg; **Fig. 7f**). Remarkably, *Cish*$^{-/-}$ mice treated with anti-PD-1 and anti-CTLA-4 developed even fewer metastases than *Cish*$^{-/-}$ mice treated with cIg (**Fig. 7f**), highlighting the potential therapeutic benefit that could be achieved if anti-CTLA-4 and anti-PD-1 therapy was combined with loss of CIS function.

CIS-deficiency promotes immunity against breast cancer metastasis

Historically, breast cancer was viewed as being immunologically silent, however, CD8^{+} T cell infiltration correlates favorably with disease outcome in triple negative breast cancers (TNBCs) and anti-PD-1 phase I clinical trials in TNBC have some indication of efficacy[29]. To examine the role of CIS checkpoint induction in breast cancer metastasis we utilized both experimental and spontaneous E0771 breast cancer metastasis models. When breast cancer cells (E0771-mCherry) were administered i.v to *Cish*$^{+/+}$, *Cish*$^{-/-}$ and NK cell-null mice, we observed a reduced tumor burden in the lungs of *Cish*$^{-/-}$ mice compared to *Cish*$^{+/+}$ and NK-null mice (**Fig. 8a, b** and **Supplementary Fig. 7c**). Histological analysis of lungs from these mice revealed the occasional

E0771 micro-metastasis in *Cish*$^{-/-}$ mice, yet they were devoid of the large metastases frequently observed around blood vessels and enriched in the visceral pleura of *Cish*$^{+/+}$ mice (**Fig. 8a**). The growth of orthotopic E0771.LMB tumors implanted in the mammary fat pad was also significantly impaired in *Cish*$^{-/-}$ mice compared to *Cish*$^{+/+}$ mice (**Fig. 8c**). When similarly sized primary orthotopic tumors (**Fig. 8d**) were surgically resected, *Cish*$^{+/+}$ mice developed spontaneous E0771.LMB metastases in the lung, whereas very few *Cish*$^{-/-}$ mice developed detectable metastases (**Fig. 8e, f** and **Supplementary Fig. 7d**), further evidence that CIS is an important negative regulator of metastatic anti-tumor immunity.

DISCUSSION

CIS has previously been shown to interact with the IL-2Rβ[21] and the elevated IL-2Rβ expression in *Cish*$^{-/-}$ NK cells is consistent with CIS targeting the IL-2Rβ for degradation. The relative contribution to the increase in IL-15-JAK-STAT signaling, will depend on whether other receptor components (IL-15Rα or γ) are limiting. Although CIS interacted with JAK1 and JAK3 activation loop peptides it preferentially inhibited JAK1 activity. Despite this selectivity, JAK3 levels were increased in *Cish*$^{-/-}$ NK cells. This may be a result of CIS directly targeting JAK3 for proteasomal degradation or alternatively, the entire receptor complex, including the associated JAK1 and 3 kinases, may be sent to the proteasome. It seems most likely that these events are not mutually exclusive, but rather that CIS has multiple targets (IL-2Rβ and JAK1) and mechanisms of action (E3 ligase activity, kinase inhibition).

Aged *Cish*$^{-/-}$ mice develop an inflammatory lung condition associated with perturbed IL-4-STAT6 and IL-2-STAT5 signaling in CD4^{+} T cells[22], whereas a recent report suggested that antigen receptor signaling was enhanced in *Cish*$^{-/-}$ CD8^{+} T cells[23]. However, adult *Cish*$^{-/-}$ mice showed no pathology or alteration in T cell frequencies[22] and in our hands, *Cish*$^{-/-}$ CD8^{+} T cell development and antigen-specific responses to MCMV were normal. Given that *Cish*$^{-/-}$ mice remain healthy, our observations suggest that antagonizing CIS therapeutically would be unlikely to have any major side effects.

Severe off-target effects and drug resistance currently limit our use of conventional chemotherapies. Consequently, there is an unmet need to find new, targeted therapies and immunotherapies that can be used in combination and as an adjunct to chemotherapy. Ipilimumab is an antibody-based therapy that targets CTLA-4 on effector and regulatory T cells and is approved for the treatment of advanced malignant melanoma, affording 10-12% tumor responses with some complicating immune-related adverse events[30,31]. Antibodies which recognize PD-1 (expressed on T cells and NK cells) or its ligand, PD-L1 (expressed on many tumors once T cell activation has occurred), are already producing 20-50% objective response rates in phase I/II trials in advanced

melanoma, renal cancer, non-small cell lung cancer (NSCLC), and other cancer indications[32-34].

Despite these advances, some cancers show less impressive responses and there remain a large number of patients where anti-CTLA-4 and anti-PD-1-PD-L1 combinations will fail. The success of cytokine therapies such as IL-2 and IL-15, which drive both NK and T cell expansion and activation, has been limited by systemic toxicity[13], whilst the adoptive transfer of autologous or haploidentical NK cells is limited by their short half-life and suppression of NK cell activity in the tumor micro-environment[36]. Combining blockade of the inhibitory receptor CD96[37,38] with CIS inhibition could further boost NK cell activity and enhance protection against tumor metastasis. Similarly, combination therapy consisting of CIS antagonism and low dose IL-15 has the potential to increase NK cell function without systemic toxicity.

In summary, IL-15-induced CIS accumulation in NK cells acts as a potent intracellular immune checkpoint that restricts NK cell function. Ablation of CIS releases a brake on NK cell activity, preventing experimental tumor metastasis and showing greater efficacy than that observed with CTLA-4-PD-1 blockade. Our results reveal CIS as a novel NK cell checkpoint and suggest that therapeutic inhibition of CIS in patients or in adoptively transferred NK cells could improve the prognosis of certain cancers.

ACCESSION CODES: GSE79409

ACKNOWLEDGEMENTS

This work is supported by program and project grants from the National Health and Medical Research Council (NHMRC) of Australia (1027472 to SC, NDH and GTB, 1013667, 1098960 to MJS, 1047903 to GTB, 1016647 to JGZ, SEN and WSA, 1049407, 1066770, 1057852 to NDH, 1078763 to DHDG), as well as an NHMRC Independent Research Institute Infrastructure Support scheme grant and a Victorian State Government Operational Infrastructure Scheme grant. NDH is a recipient of a Melanoma Research Grant from the Harry J Lloyd Charitable Trust and RBD is supported by a Leukemia Foundation scholarship. This work is also supported by fellowships from the NHMRC (GNT0461276 to NDH, 1058344 to WSA, 545952 to DSH, 1090236 to DHDG, 1089072 to CT, Australia Fellowship 1078671 to MJS), the Australian Research Council (GTB), and the Menzies Foundation (NDH). EMP is supported by a Schroedinger Fellowship from the Austrian Science Fund (FWF): J-3635. The SGC is a registered charity (number 1097737) that receives funds from AbbVie, Bayer PHARMA AG, Boehringer Ingelheim, the Canada Foundation for Innovation, the Canadian Institutes for Health Research, Genome Canada, GlaxoSmithKline, Janssen, Lilly Canada, the Novartis Research Foundation, the Ontario Ministry of Economic Development and Innovation, Pfizer, Takeda, and the Wellcome Trust [092809/Z/10/Z]. We wish to thank Nicos Nicola for helpful comments and discussion, Patricia Rueda and Cathy Quillici for technical assistance, Tracy Wilson for generating the wild-type and SH2-mutant CIS expression plasmids, Robin Anderson for the E0771.LMB cells and Liam Town, Kate Elder, Tania Camilleri and Joanne Sutton for excellent animal husbandry. We are grateful to the staff of the WEHI Bioservices, Monoclonal antibody facility, Flow cytometry facility and Clinical Translational Centre.

AUTHOR CONTRIBUTIONS:

RBD, TBK, LFD, JR, WS, EP, DSH, KS, JGZ, KS, MF, TU, CEA, PPS, CES, GI, NPDL, EML, CS, DH, AIW, JJB, SSL, ANB, SEN and NDH all performed experiments. MAP, CJB, WSA, GTB, SC, DHDG and MJS provided key reagents and scientific input into experimental design and interpretation of the results. MJS, JJB, SEN and NDH supervised experimental design and provided input into interpretation of results and writing of the paper.

COMPETING FINANCIAL INTERESTS STATEMENT: M.J.S. has been supported by a scientific research agreement with Bristol Myers Squibb and Medimmune and is a consultant for Kymab, F-star, and AMGEN.

REFERENCES

1 Hanahan, D. & Weinberg, R. A. Hallmarks of cancer: the next generation. *Cell* **144**, 646-674, doi:10.1016/j.cell.2011.02.013 (2011).

2 Schreiber, R. D., Old, L. J. & Smyth, M. J. Cancer immunoediting: integrating immunity's roles in cancer suppression and promotion. *Science* **331**, 1565-1570, doi:10.1126/science.1203486 (2011).

3 Tumeh, P. C. *et al.* PD-1 blockade induces responses by inhibiting adaptive immune resistance. *Nature* **515**, 568-571, doi:10.1038/nature13954 (2014).

4 Ho, P. C. *et al.* Phosphoenolpyruvate Is a Metabolic Checkpoint of Anti-tumor T Cell Responses. *Cell* **162**, 1217-1228, doi:10.1016/j.cell.2015.08.012 (2015).

5 Shin, D. S. & Ribas, A. The evolution of checkpoint blockade as a cancer therapy: what's here, what's next? *Current opinion in immunology* **33**, 23-35, doi:10.1016/j.coi.2015.01.006 (2015).

6 Restifo, N. P., Smyth, M. J. & Snyder, A. Acquired resistance to immunotherapy and future challenges. *Nature reviews. Cancer* **16**, 121-126, doi:10.1038/nrc.2016.2 (2016).

7 Vivier, E., Ugolini, S., Blaise, D., Chabannon, C. & Brossay, L. Targeting natural killer cells and natural killer T cells in cancer. *Nature reviews. Immunology* **12**, 239-252, doi:10.1038/nri3174 (2012).

8 Huntington, N. D., Vosshenrich, C. A. & Di Santo, J. P. Developmental pathways that generate natural-killer-cell diversity in mice and humans. *Nature reviews. Immunology* **7**, 703-714, doi:10.1038/nri2154 (2007).

9 Huntington, N. D. The unconventional expression of IL-15 and its role in NK cell homeostasis. *Immunology and cell biology* **92**, 210-213, doi:10.1038/icb.2014.1 (2014).

10 Verdeil, G., Puthier, D., Nguyen, C., Schmitt-Verhulst, A. M. & Auphan-Anezin, N. STAT5-mediated signals sustain a TCR-initiated gene expression program toward differentiation of CD8 T cell effectors. *Journal of immunology* **176**, 4834-4842 (2006).

11 Huntington, N. D. *et al.* Interleukin 15-mediated survival of natural killer cells is determined by interactions among Bim, Noxa and Mcl-1. *Nature immunology* **8**, 856-863, doi:10.1038/ni1487 (2007).

12 Sathe, P. *et al.* Innate immunodeficiency following genetic ablation of Mcl1 in natural killer cells. *Nature communications* **5**, 4539, doi:10.1038/ncomms5539 (2014).

13 Floros, T. & Tarhini, A. A. Anticancer Cytokines: Biology and Clinical Effects of Interferon-alpha2, Interleukin (IL)-2, IL-15, IL-21, and IL-12. *Seminars in oncology* **42**, 539-548, doi:10.1053/j.seminoncol.2015.05.015 (2015).

14 Hilton, D. J. *et al.* Twenty proteins containing a C-terminal SOCS box form five structural classes. *Proc Natl Acad Sci U S A* **95**, 114-119 (1998).

15 Linossi, E. M., Babon, J. J., Hilton, D. J. & Nicholson, S. E. Suppression of cytokine signaling: the SOCS perspective. *Cytokine & growth factor reviews* **24**, 241-248, doi:10.1016/j.cytogfr.2013.03.005 (2013).

16 Zhang, J. G. *et al.* The conserved SOCS box motif in suppressors of cytokine signaling binds to elongins B and C and may couple bound proteins to proteasomal degradation. *Proc Natl Acad Sci U S A* **96**, 2071-2076 (1999).

17 Yasukawa, H. *et al.* The JAK-binding protein JAB inhibits Janus tyrosine kinase activity through binding in the activation loop. *EMBO J* **18**, 1309-1320, doi:10.1093/emboj/18.5.1309 (1999).
18 Kershaw, N. J. *et al.* SOCS3 binds specific receptor-JAK complexes to control cytokine signaling by direct kinase inhibition. *Nature structural & molecular biology* **20**, 469-476, doi:10.1038/nsmb.2519 (2013).
19 Yoshimura, A. *et al.* A novel cytokine-inducible gene CIS encodes an SH2-containing protein that binds to tyrosine-phosphorylated interleukin 3 and erythropoietin receptors. *Embo J* **14**, 2816-2826 (1995).
20 Matsumoto, A. *et al.* CIS, a cytokine inducible SH2 protein, is a target of the JAK-STAT5 pathway and modulates STAT5 activation. *Blood* **89**, 3148-3154. (1997).
21 Aman, M. J. *et al.* CIS associates with the interleukin-2 receptor beta chain and inhibits interleukin-2-dependent signaling. *The Journal of biological chemistry* **274**, 30266-30272 (1999).
22 Yang, X. O. *et al.* The signaling suppressor CIS controls proallergic T cell development and allergic airway inflammation. *Nature immunology* **14**, 732-740, doi:10.1038/ni.2633 (2013).
23 Palmer, D. C. *et al.* Cish actively silences TCR signaling in CD8+ T cells to maintain tumor tolerance. *The Journal of experimental medicine* **212**, 2095-2113, doi:10.1084/jem.20150304 (2015).
24 Burns, C. J., Segal, D. & Wilks, A. F. in *JAK-STAT Signalling Methods and Protocols* (eds S.E. Nicholson & N. A. Nicola) Ch. 7, 99-112 (Human Press, USA, 2013).
25 Mlecnik, B. *et al.* Functional network pipeline reveals genetic determinants associated with in situ lymphocyte proliferation and survival of cancer patients. *Science translational medicine* **6**, 228ra237, doi:10.1126/scitranslmed.3007240 (2014).
26 Davies, H. *et al.* Mutations of the BRAF gene in human cancer. *Nature* **417**, 949-954, doi:10.1038/nature00766 (2002).
27 Larkin, J. *et al.* Combined Nivolumab and Ipilimumab or Monotherapy in Untreated Melanoma. *The New England journal of medicine* **373**, 23-34, doi:10.1056/NEJMoa1504030 (2015).
28 Postow, M. A. *et al.* Nivolumab and ipilimumab versus ipilimumab in untreated melanoma. *The New England journal of medicine* **372**, 2006-2017, doi:10.1056/NEJMoa1414428 (2015).
29 Homet Moreno, B. & Ribas, A. Anti-programmed cell death protein-1/ligand-1 therapy in different cancers. *British journal of cancer* **112**, 1421-1427, doi:10.1038/bjc.2015.124 (2015).
30 Hodi, F. S. *et al.* Improved survival with ipilimumab in patients with metastatic melanoma. *The New England journal of medicine* **363**, 711-723, doi:10.1056/NEJMoa1003466 (2010).
31 Robert, C. *et al.* Ipilimumab plus dacarbazine for previously untreated metastatic melanoma. *The New England journal of medicine* **364**, 2517-2526, doi:10.1056/NEJMoa1104621 (2011).
32 Brahmer, J. R. *et al.* Safety and activity of anti-PD-L1 antibody in patients with advanced cancer. *The New England journal of medicine* **366**, 2455-2465, doi:10.1056/NEJMoa1200694 (2012).
33 Topalian, S. L. *et al.* Safety, activity, and immune correlates of anti-PD-1 antibody in cancer. *The New England journal of medicine* **366**, 2443-2454, doi:10.1056/NEJMoa1200690 (2012).
34 Herbst, R. S. *et al.* Predictive correlates of response to the anti-PD-L1 antibody MPDL3280A in cancer patients. *Nature* **515**, 563-567, doi:10.1038/nature14011 (2014).
35 Wolchok, J. D. *et al.* Nivolumab plus ipilimumab in advanced melanoma. *The New England journal of medicine* **369**, 122-133, doi:10.1056/NEJMoa1302369 (2013).

36 Knorr, D. A., Bachanova, V., Verneris, M. R. & Miller, J. S. Clinical utility of natural killer cells in cancer therapy and transplantation. *Seminars in immunology* **26**, 161-172, doi:10.1016/j.smim.2014.02.002 (2014).
37 Chan, C. J. *et al.* The receptors CD96 and CD226 oppose each other in the regulation of natural killer cell functions. *Nature immunology* **15**, 431-438, doi:10.1038/ni.2850 (2014).
38 Blake, S. J. *et al.* Suppression of metastases using a new lymphocyte checkpoint target for cancer immunotherapy. *Cancer discovery*, doi:10.1158/2159-8290.CD-15-0944 (2016).

FIGURE LEGENDS

Figure 1. CIS-deficient NK cells display superior proliferation, survival and killing in response to IL-15

(a) Quantitative PCR analysis of SOCS-encoding mRNA (vertical axis) in wild-type NK cells incubated for 0-24 h (horizontal axes) with IL-15 (50 ng/ml). **(b)** Immunoblotting for CIS and STAT3 in NK cells treated as in (a). **(c)** Flow cytometry enumerating NK cells ($NK1.1^+NKp46^+TCR\text{-}\beta^-$) in bone marrow (BM), liver, lung and spleens of wild-type ($Cish^{+/+}$) and *Cish*-deficient ($Cish^{-/-}$) mice. **(d)** Flow cytometric analysis of NK1.1 and NKp46 expression on $Cish^{+/+}$ and $Cish^{-/-}$ splenic NK cells. MFI: mean fluoresence index **(e)** Flow cytometric analysis of $Cish^{+/+}$ and $Cish^{-/-}$ NK cells labeled with CFSE and CTV, respectively, mixed and cultured at a ratio of 1:1 for 5 days in IL-15 (5-40 ng/ml). (**f**) Flow cytometric analysis of IFN-γ production and CD107a (LAMP-1) expression in $Cish^{+/+}$ and $Cish^{-/-}$ NK cells cultured for 4 h in IL-15 with either an immunoglobulin control (cIg), anti-NK1.1, anti-NKp46 or anti-Ly49H (confers anti-viral response) antibodies or IL-12 and IL-18 (positive control). *p<0.05, using a Mann-Whitney U test. (**g**) Cytotoxicity of $Cish^{+/+}$ and $Cish^{-/-}$ NK cells against CHO target cells at the indicated NK:CHO (E:T; Effector:Target) ratios. Normalized CHO Cell Index (vertical axis) was determined by xCELLigence. (**a**; n=3 biological replicates. **b**; one representative of two immunoblots. **c, d**; n=6 biological replicates. **e**; one representative of 3 experiments. **f**; values indicate percentage for one representative of two experiments with n=3 biological replicates. **g**; n=3 technical replicates of a representative experiment of two independent experiments. **a, g**; mean and s.d. **c, d**; mean and s.e.m.)

Figure 2. CIS-deficient NK cells display extensive transcriptional changes in response to IL-15
Quantitative RNA transcript analysis (vertical axis; reads per kilobase of exon per million reads) of *in vitro*-derived $Cish^{+/+}$ and $Cish^{-/-}$ NK cells was performed by RNA sequencing. Selected genes differentially expressed in $Cish^{-/-}$ NK cells are shown. n=2 biological replicates. See also **Supplementary Fig. 4.**

Figure 3. CIS negatively regulates IL-15 signaling by targeting JAK-STAT signaling

(a) Flow cytometric analysis of IL-2Rβ (CD122) surface expression (MFI; mean fluorescence index) on naive and IL-15 cultured *ex vivo* $Cish^{+/+}$ and $Cish^{-/-}$ NK cells. *$p \leq 0.01$; ** $p \leq 0.001$ using a Mann-Whitney U test. **(b)** Immunoblot analysis of *ex vivo* $Cish^{+/+}$ and $Cish^{-/-}$ NK cells incubated *in vitro* with 50 ng/ml IL-15 for the indicated times. **(c)** Alternatively, $Cish^{+/+}$ and $Cish^{-/-}$ NK cells derived from 7-10 day IL-15 cultures were washed free of cytokine and rested for 4 h prior to IL-15 treatment. Cells were lysed and analyzed by immunoblotting with antibodies to the indicated phosphorylated (p) and total proteins. **(d)** Immunoblot analysis of $Cish^{+/+}$ and $Cish^{-/-}$ NK cells cultured in IL-15 and washed free of cytokine-containing media prior to lysis at various times post-wash. (**a**; *n*=6 biological replicates, mean and s.e.m.) (**c**; one experiment representative of three independent experiments with similar results).

Figure 4. *Cish*$^{-/-}$ NK cells have increased active kinase levels following IL-15 stimulation

(a) Mass spectrometric analysis of JAK kinases enriched from NK cell lysates generated as in Fig. 3c using a modified N-linker analogue of the JAK inhibitor CYT387 coupled to NHS-sepharose beads. Enriched kinases were eluted and digested with trypsin prior to mass spectrometry. Summed JAK1 and JAK3 peptide intensities are shown from $Cish^{+/+}$ and $Cish^{-/-}$ NK cells. *$p \leq 0.01$. **(b)** Volcano plot shows the Log2 protein ratios following the quantitative pipeline analysis ($Cish^{-/-}$ NK cell lysate relative to $Cish^{+/+}$). Proteins with a –log10 $p \geq 1.3$ were deemed differentially expressed. **(c)** Heat map of summed peptide intensities (non-imputed, Log2-transformed) for significantly altered kinases shown for each independent replicate. Gene Ontology analysis revealed an enrichment of kinases involved in cell cycle and DNA replication in $Cish^{-/-}$ NK cells. (**a, b, c**; *n*=3 biological replicates). See also **Supplementary Table 1**. See also **Supplementary Fig. 5**.

Figure 5. CIS-SH2 domain binds to the JAK activation loop targeting JAK1 for proteasomal degradation.

(a and b) Immunoblot analysis of anti-FLAG immunoprecipitates (upper panels) and cell lysates (lower panels) from 293T cells expressing FLAG-tagged JAK1 and JAK3 together with Flag-tagged-CIS, SOCS1, SOCS3 or CIS mutants in which the SH2 domain (H; R107K) or the Cullin-5 binding site in the SOCS box had been mutated (B; P241A/L242A/P243A). In some instances, cells were treated with the proteasome inhibitor, MG132. (p=phosphorylated). **(c)** Anti-FLAG immunoblot of anti-CIS (upper left panel) or anti-JAK1 immunoprecipitates (upper right panel) from 293T cells co-expressing FLAG-tagged CIS and JAK1. Protein expression is shown in the lower panels by anti-FLAG blot of cell lysates (JAK1: left panel; CIS: right panel). **(d)** Anti-phosphorylated (p) JAK1 immunoblot of samples following *in vitro* ubiquitination reaction. FLAG-JAK1 was incubated with the CIS-E3 ligase complex (CIS-SH2-BC with Cullin5 and Rbx2), together with ubiquitin, E1 and E2 enzymes at 37^{o}C for the times indicated. Data are from one experiment representative of two independent experiments with similar results (**a-c**) or three experiments (**d**).

Figure 6. CIS-SH2 binding specifically inhibits JAK1 kinase activity.

(a) Immunoblot analysis of cultured wild-type NK cells washed and starved of IL-15 for 4 h, with and without addition of the proteasomal inhibitor and then stimulated for the indicated times with 50 ng/ml IL-15. (p=phosphorylated) **(b)** *In vitro* kinase assay performed with the kinase domain (JH1) of all four JAKs and the CIS-SH2 domain (SH2-SB-BC complexes). **(c)** *In vitro* kinase assay performed with the JAK1 kinase domain (JH1) and the SH2-domains of CIS, SOCS1, SOCS2 or SOCS3 (SH2-SB-BC complexes). **(b and c)** Data were normalized to no-CIS/SOCS controls. % JAK kinase activity (vertical axis), SOCS protein concentration (horizontal axis). Data shown are the average and range of technical duplicates and are representative of 3-5 independent experiments.

Figure 7. Loss of CIS checkpoint induction in NK cells reduces experimental lung metastasis.

Metastatic burden (vertical axis) in the lungs of *Cish*$^{+/+}$ and *Cish*$^{-/-}$ mice 14 days following i.v injection of **(a)** B16F10 melanoma cells, (**b**) LWT1 (B-RAF mutant) melanoma or **(c)** RM-1 prostate carcinoma cells. **p<0.005, ***p<0.0001 **(d)** Metastatic burden (vertical axis) in the lungs of *Cish*$^{+/+}$ and *Cish*$^{-/-}$ mice treated with either control immunoglobulin (cIg), anti-CD8 (αCD8; CD8^{+} T cell depletion), anti-asialoGM1 (αasGM1; NK cell depletion) or anti-IFN-γ (αIFN-

γ; neutralising) antibodies on days -1, 0 and 6 relative to B16F10 melanoma injection. *p<0.05 **(e)** Metastatic burden (vertical axis) in the lungs of NK cell-deficient (*Ncr1*$^{Mcl1\Delta/\Delta}$) mice injected with B16F10 melanoma cells and either *Cish*$^{+/+}$ or *Cish*$^{-/-}$ NK cells or PBS. *p<0.05. **(f)** Metastatic burden (vertical axis) in the lungs of *Cish*$^{+/+}$ and *Cish*$^{-/-}$ mice 13 days following B16F10 melanoma injection. On days 0, 3 and 6 relative to tumor inoculation, mice received either control Ig or combination anti-PD-1 and anti-CTLA-4 antibodies. **p<0.005. (**a-f;** mean and s.e.m of indicated n). p values were determined by (**a-d, f**) a Mann-Whitney U test or (**e**) unpaired student's t-test. See also **Supplementary Fig. 7.**

Figure 8. CIS-deficiency protects against experimental and spontaneous breast cancer metastasis. Metastatic burden in the lungs of *Cish*$^{+/+}$, *Cish*$^{-/-}$ and *Ncr1*$^{Mcl1\Delta/\Delta}$ (NK-null) mice injected i.v. with E0771-mCherry^{+}luciferase^{+} breast cancer cells was analyzed by (**a**) H&E stained histological sections or (**b**) *In vivo* imaging (IVIS) of mCherry+ fluoresence (vertical axis: total radiant efficiency [(p/s)/ ÌW/cm^2)]x1e^7). (**c**) Growth of orthotopic E0771.LMB-mCherry^{+} breast cancer cells implanted into the mammary fat pad of *Cish*$^{+/+}$ and *Cish*$^{-/-}$ mice (vertical axis; tumor volume). E0771.LMB tumors generated as in **(c)** were surgically removed at 400–600 mm^3 and weighed post-excision **(d).** Spontaneous lung metastases were measured 14 days later by **(e)** RT-PCR for mCherry mRNA expression and **(f)** IVIS for mCherry fluorescence (vertical axis: total radiant efficiency [(p/s)/ ÌW/cm^2)]x1e^7). (**b, d-f**; mean and s.e.m of indicated n). *p<0.05, values were determined by (**b**) Mann-Witney U test or (**c-f**) unpaired students's t-test. See also **Supplementary Fig. 7.**

Table 1. Isothermal calorimetry (ITC) showing binding affinity of hCIS-SH2-BC to phosphopeptides corresponding to tyrosines within the JAK1 and 3 kinase domain activation loops and IL-2Rβ cytoplasmic domains.

Ligand	K_D (μM)	ΔH (kcal/mol)	Sequence
JAK1 (pY1034)	2.1 ± 1.0*	-2.5 ± 0.4*	AIETDKE**pY**YTVKDDRD
JAK3 (pY980)	0.8 ± 0.5	-2.8 ± 0.5	LLPLDKD**pY**YVVREPGQ
JAK1 (Y1034)	>10	N.D.	AIETDKEYYTVKDDRD
IL-2Rβ (pY338)	7.0 ± 2	-2.7 ± 0.3	NGQ**pY**FFFHLPDA
IL-2Rβ (pY355)	0.94 ± 0.3	-5.4 ± 0.9	CQV**pY**FTYDPYSE
IL-2Rβ (pY361)	1.5 ± 0.2	-6.3 ± 0.4	YDP**pY**SEEDPDEG
IL-2Rβ (pY392)	1.8 ± 0.7	-3.5 ± 0.3	DDA**pY**CTFPSRDD

*Average and range from two independent experiments. N.D.=Not detectable, p=phosphorylated.

ONLINE METHODS

Mice

Cish$^{-/-}$ were generously provided by J. Ihle and E. Parganas at St. Jude Children's Research Hospital, Memphis USA and were maintained on a C57BL/6 background[23]. *Cish*$^{+/+}$ refers to C57BL/6 wild-type control mice. *Rosa26-CreERT2* (TaconicArtemis), *Socs3-loxP*[39], *Ifng*$^{-/-}$ *Socs1*$^{-/-}$[40] and *Ncr1-iCre*[41] mice have been described previously. Male and female mice were used between the ages of 6-14 weeks. Age and sex matched mice were used and cohort size was dictated by previous experience using these tumor models. Sex discrimination was employed for the E0771 breast cancer model as females were essential. All mice were bred and maintained at the Walter and Eliza Hall Institute. Animal experiments followed the National Health and Medical Research Council (NHMRC) Code of Practice for the Care and Use of Animals for Scientific Purposes guidelines and were approved by the Walter and Eliza Hall Institute Animal Ethics Committee or the QIMR Berghofer Medical Research Institute Animal Ethics Committee or the Animal Ethics and Experimentation Committee of the University of Western Australia.

Purification and culture of NK cells

Murine natural killer cells were harvested from various organs (spleen, bone marrow, blood) and single-cell suspensions prepared by forcing of organs through 70 μM sieves. Lymphocytes were isolated from liver by suspension in isotonic percoll (Amersham Pharmacia Biotech) and centrifugation at 1800 x *g*. NK cells were purified using anti-CD49b (DX5) Microbeads (Miltenyi Biotec) according to manufacturer's specifications. NK cells were expanded for 5-10 days by culture in Iscove's modified Dulbecco's medium (IMDM) supplemented with 10% (v/v) foetal calf serum (FCS), L-glutamine (1 mM; Gibco), streptomycin (100 μg/mL; Sigma), penicillin (100 IU/ml; Sigma), gentamycin (50 ng/ml; Sigma) and recombinant hIL-15 (50 ng/ml; Peprotech).

RNA sequencing and bioinformatic analysis

100 base pair single-end RNA sequencing was performed for two biological replicates of 1x10^6 *Cish*$^{+/+}$ and *Cish*$^{-/-}$ NK1.1$^+$NKp46$^+$TCRb$^-$ NK cells grown in 50 ng/ml IL-15 for 7 days and two biological replicates of 1x10^6 freshly isolated *Cish*$^{+/+}$ and *Cish*$^{-/-}$ NK1.1$^+$NKp46$^+$TCRβ$^-$ NK cells using the Illumina HiSeq2000 at the Australia Genomic Research Facility, Melbourne. Accession code: GSE79409. Reads were aligned to the GRCm38/mm10 build of the *Mus musculus* genome using the Subread aligner. Genewise counts were obtained using FeatureCounts. Reads overlapping exons in annotation build 38.1 of NCBI RefSeq database were included. Genes were filtered from

downstream analysis if they failed to achieve a CPM (counts per million mapped reads) value of at least 0.5 in at least two libraries. Counts were converted to log2 counts per million, quantile normalized and precision weighted with the voom function of the limma package. Linear models and empirical bayes methods were used to assess differential expression in RNAseq experiments. Genes were called differentially expressed if they achieved a false discovery rate of 0.1 or less and also had at least 8 FPKMs (fragments per kilobases per million mapped reads) in one or both of the two cell types being compared. Heat maps were generated using the gplots package, with negative log2 FPKM values reset to zero. All analyses were carried out using Bioconductor R packages.

***In vitro* NK cell proliferation assays**

Cultured NK cells from *Cish*$^{+/+}$ and *Cish*$^{-/-}$ mice were incubated with 0.1 nM carboxyfluorescein succinimidyl ester (CFSE) and cell tracker violet (CTV; Life Technologies), respectively. Labeled NK cells were then co-cultured (1x10^5 of each) *in vitro* with various doses of hIL-15 for 5 days, prior to analysis by flow cytometry.

Murine cytomegalovirus (MCMV) infection

Mice were injected intraperitoneally with 5x10^3 plaque forming units (PFU) of salivary gland-propagated virus stock of MCMV-K181-Perth strain diluted in phosphate buffered saline (PBS) containing 0.5% FCS. At day 7 post-infection spleens were removed and leukocytes prepared according to standard protocols. Mixed bone marrow chimeras were generated by reconstituting lethally irradiated Ly5.1$^+$5.2$^+$ hosts with 5x10^6 *Cish*$^{+/+}$Ly5.1$^+$ and 5x10^6 *Cish*$^{-/-}$ Ly5.2$^+$ total bone marrow cells. Antibodies used for flow cytometry were purchased from BD Biosciences (San Diego, CA) or eBioscience (San Diego, CA). Phycoerythrin-conjugated tetramers for m45 and m38 were purchased from ImmunoID (Melbourne, Victoria).

Xcelligence assays

Target cells (CHO, B16F10) were seeded into the wells of 96X E-Plates in 100 µl of media. Cell growth was dynamically monitored with the impedance-based RT-CES® system until they reached log growth phase and formed a monolayer (approximately 24 h). Cultured *Cish*$^{+/+}$ and *Cish*$^{-/-}$ NK cells at different concentrations were then added directly to individual wells containing the target cells. For background controls, NK cells were added to wells that contained no target cells, and target cells were added to wells without the addition of NK cells. After addition of NK cells, the system continued to take measurements every 15 min for up to 48 h.

Flow cytometry and cell sorting

Single-cell suspensions were stained with the appropriate monoclonal antibody in PBS containing 2% (v/v) FCS. When necessary, intracellular staining was performed by use of the FoxP3/Transcription Factor Staining Buffer Set (eBioscience) according to the manufacturer's instructions. FACS Verse, Fortessa and AriaII (BD Biosciences) were used for cell sorting and analysis, with dead cells excluded by propidium iodide or Fluoro-Gold staining. All single cell suspensions were diluted in PBS prior to analysis and enumerated using the Advia hematology analyzer (Siemens). Antibodies specific for NK1.1 (PK136; 1:100), CD19 (1D3; 1:500), CD3 (17A2; Biolegend; 1:400) CD122 (TM-b1; 1:200), CD3 (145-2C11; 1:100), CD8 (53-6.7; 1:200), CD132 (4G3; 1:200), NKp46 (29A1.4; 1:100), TCR-β (H57-5921; 1:500), KLRG1 (2F1; 1:100), CD27 (LG.7F9; 1:200), FoxP3 (FJK-16s; eBioscience; 1:400), CD25 (PC61; BioLegend; 1:100), Sca-1 (D7; 1:100), B220 (RA3-6B2; eBioscience; 1:100), Gr-1 (1A8; 1:200), Granzyme A (GzA-3G8.5; eBioscience; 1:200), Granzyme B (NGZB; eBioscience; 1:200), CD107a (104B; 1:100) and IFN-γ (XMG1.2; 1:100) were from BD Pharmingen unless stated otherwise. M45 and m38 tetramers were purchased from ImmunoID (Melbourne, Victoria) and used at 1:100.

IL-2 *in vivo* expansion of innate lymphocyte cells (ILC2) and regulatory T cells (T_{regs})

IL-2 in complex with specific anti-IL-2 antibodies can lead to expansion of different T cells subsets[42]. Here we have used IL-2 in complex with the JES6-1 antibody to selectively expand ILC2 and T_{regs} *in vivo*. *Cish*$^{+/+}$ and *Cish*$^{-/-}$ mice were injected i.p. daily with IL-2 complexed with anti-IL-2 antibodies (5µg JES6.1 + 1 µg IL-2) for 5 days and ILC2 and Tregs analyzed by flow cytometry.

Real-time quantitative PCR (Q-PCR)

Total RNA was isolated using the RNeasy plus kit (QIAGEN) and cDNA synthesis performed with Superscript III (Invitrogen) according to the manufacturer's instructions. PCR reactions were performed in 10 µL; 5 µL of FastStart SYBR Green Master Mix (Roche), 0.5 pmol of forward and reverse primers and 4 µL of cDNA. Primer sequences and PCR conditions have been described[43]. Real-time Q-PCR was performed on an ABI Prism 7900HT sequence detection system (Applied Biosystems). mRNA levels were quantified against standard curves generated using sequential dilutions of an oligonucleotide corresponding to each amplified PCR fragment and using SDS2.2 software (Applied Biosystems). Relative expression was determined by normalizing the amount of each gene of interest to the housekeeping gene Glyceraldehyde-3-Phosphate Dehydrogenase (GAPDH). Each condition had three biological replicates and measurements were performed in duplicate. Statistical analysis was performed using an unpaired t-test with a 95% confidence level.

Immunoblotting and transient transfections

NK cells were lysed in KALB lysis buffer[44] supplemented with protease inhibitors (Complete Cocktail tablets, Roche), 1 mM PMSF, 1 mM Na_3VO_4 and 1 mM NaF and incubated for 1 h on ice. Lysates were clarified by centrifugation at 16,060 x g for 15 min at 4° C. Protein concentrations were determined by the BCA method (Pierce, Rockford). 293T cells were maintained in DMEM supplemented with 100 U/mL penicillin, 0.1 ng/ml streptomycin and 10% FCS and were transiently transfected with vector alone or cDNA expressing Flag-tagged mouse *Jak1*, *Jak3*, *Cish* or *Cish* mutants or Myc-tagged mouse *Cish*, using FuGene6 (Promega) according to the manufacturer's instructions. In some instances, cells were pre-treated with 10 μM MG132 for 4 h to block proteasomal degradation. 48 h post-transfection cells were lysed in KALB buffer[44]. FLAG proteins were immunoprecipitated using M2-beads (Sigma) and proteins eluted in SDS sample buffer. Immunoprecipitation, gel electrophoresis and immunoblotting were performed essentially as described[45]. The following primary antibodies were used: antibodies to CIS (Clone D4D9), phospho-STAT3 (Y705); phospho-AKT1 (Ser473), AKT and MAPK were obtained from Cell Signaling Technology. Antibodies to phospho-STAT5A/B (Y694/699) were from Millipore, phospho-JAK1 (Y1022/1023) and STAT5A from Invitrogen, and JAK1, STAT3 and β-Actin were obtained from Santa Cruz Biotechnology Inc. Rat anti-Flag antibody was a kind gift from D. Huang & L. O'Reilly (Walter and Eliza Hall Institute).

CYT-387 analogue synthesis

Liquid chromatography mass spectroscopy (LCMS) was carried out using a Finnigan LCQ Advantage Max using reverse phase high performance liquid chromatography (HPLC) analysis (column: Gemini 3*μ* C18 20 x 4.0 mm 110A) Solvent A: Water 0.1% Formic Acid, Solvent B: Acetonitrile 0.1% Formic Acid, Gradient: 10-100% B over 10 min Detection: 100-600 nm and electrospray ionization (ESI). All compounds submitted for biochemical assay were assessed to have purity ≥ 95% as measured by HPLC analysis at 254 nm UV absorbance. Chromatography was performed using the CombiFlash® Rf purification system (Teledyne, ISCO, Lincoln, NE, USA) with pre-packed silica gel columns (particle size 0.040-0.063 mm). All commercial reagents were used as received. Cbz = carboxybenzyl. Benzyl 4-(4-aminophenyl)piperazine-1-carboxylate (**S1**) and Ethyl 4-(4-chloropyrimidin-2-yl)benzoate (**S2**) can be prepared as previously described.[i,ii]

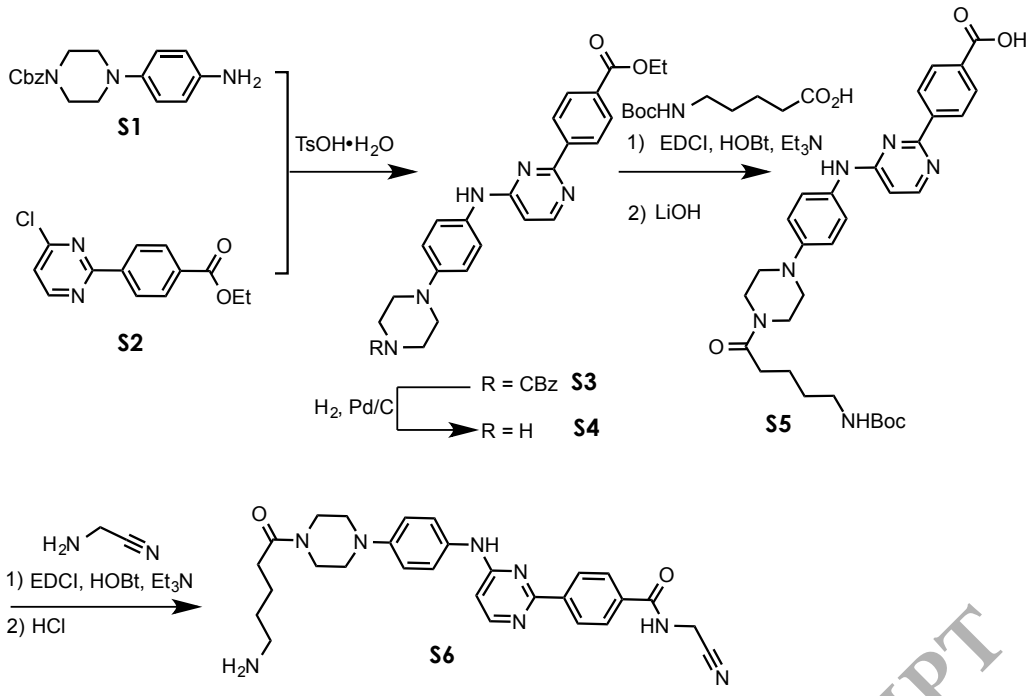

Benzyl 4-(4-((2-(4-(ethoxycarbonyl)phenyl)pyrimidin-4-yl)amino)phenyl)piperazine-1-carboxylate (S3)

p-TsOH (0.978 g, 5.13 mmol) was added to a magnetically stirred suspension of pyrimidine **S2** (1.50 g, 5.71 mmol) and aniline **S1** (2.31 g, 7.42 mmol) in dioxane (20 mL). The mixture was heated to reflux for 24 h. The mixture was cooled, diluted in DCM (250 mL) and washed with $NaHCO_3$ (100 mL) and the aqueous layer was separated and extracted with EtOAc (3 x 50 mL). The combined organics were dried (Na_2SO_4), filtered and concentrated onto silica and the material was subjected to flash chromatography (1:9 to 1:0, v/v, EtOAc:cyclohexane). The fractions thus obtained were concentrated and the yellow precipitate was filtered and washed with methanol affording the *title compound* (**S3**) (1.61 g, 52%) as a yellow solid. **^{1}H NMR** (600 MHz, DMSO-d6): δ 9.51 (s, 1H), 8.52 (d, *J* = 5.1 Hz, 1H), 8.25 (d, *J* = 8.3 Hz, 2H), 8.08 (d, *J* = 8.4 Hz, 2H), 7.65 (d, *J* = 9.0 Hz, 2H), 7.37-7.35 (m, 5H), 7.31 (q, *J* = 4.4 Hz, 1H), 6.93 (d, *J* = 9.0 Hz, 2H), 5.09 (s, 2H), 4.33 (q, *J* = 7.1 Hz, 2H), 3.58-3.48 (m, 4H), 3.04-3.03 (m, 4H), 1.33 (t, *J* = 7.1 Hz, 3H). **LCMS**: t_R = 6.14 min, m/z = 538.0 $[M+H]^+$.

Ethyl 4-(4-((4-(piperazin-1-yl)phenyl)amino)pyrimidin-2-yl)benzoate (S4)

Compound **S3** (500 mg, 0.93 mmol) was dissolved in MeOH (75 mL) and THF (50 mL) and the solution was passed through the 'H-cube' at 1 mL/min in full H_2 mode using a Pd/C (10%) cartridge at 45 ºC. The product was collected and concentrated under reduced pressure to afford the title compound (**S4**) (352 mg, 94%) as a dark solid. **^{1}H NMR** (600 MHz, $CDCl_3$): δ 8.46 (dd, *J* = 8.0, 5.2 Hz, 1H), 8.16-8.14 (m, 2H), 8.11 (d, *J* = 8.3 Hz, 2H), 7.59 (dd, *J* = 8.9, 1.9 Hz, 1H), 7.55 (d, *J* =

8.9 Hz, 1H), 7.16-7.13 (m, 1H), 6.96 (dt, *J* = 9.1, 4.6 Hz, 2H), 4.41 (q, *J* = 7.1 Hz, 2H), 3.36-3.28 (m, 4H), 3.25-3.18 (m, 4H), 1.42 (t, *J* = 7.1 Hz, 3H). **LCMS**: t_R = 5.78 min, m/z = 404.0 $[M+H]^+$.

4-(4-((4-(4-(5-((*tert*-Butoxycarbonyl)amino)pentanoyl)piperazin-1-yl)phenyl)amino)pyrimidin-2-yl)benzoic acid (S5)

To a magnetically stirred solution of *N*-Boc-aminovaleric acid (194 mg, 0.96 mmol), EDCI (201 mg, 1.05 mmol), HOBt (146 mg, 1.05 mmol), Et_3N (232 μL, 1.75 mmol) in DMF (2 mL) was added compound **S4** (350 mg, 0.87 mmol) under N_2 and the mixture was stirred for 12 h. The reaction mixture was washed with water (2 mL) and the aqueous washings were extracted with EtOAc (2 x 2 mL). The organic fractions were combined, dried (Na_2SO_4), filtered and concentrated. The crude material was purified by Flash chromatography to afford a pale yellow solid (373 mg). This material was dissolved in THF/MeOH (2 mL of a 1:3 mixture) and lithium hydroxide (123 mg, 3.09 mmol) was added and the mixture stirred at reflux for 2 h. The mixture was concentrated to yellow solid and suspended in water and acidified to pH = 2 with HCl (5% aqueous solution). The precipitate was collected by filtration, washed with MeOH (1 mL) then Et_2O (2 x 1 mL) and dried under reduced pressure affording the *title compound* (**S5**) (224 mg, 60%) as red solid. **^{1}H-NMR** (600 MHz, DMSO-d_6): δ 9.49 (s, 1H), 8.52-8.51 (m, 1H), 8.22 (t, *J* = 6.8 Hz, 2H), 8.06 (d, *J* = 8.1 Hz, 2H), 7.65-7.64 (m, 2H), 7.36 (dd, *J* = 4.7, 0.3 Hz, 1H), 6.94-6.91 (m, 2H), 6.77-6.75 (m, 1H), 3.57-3.55 (m, 4H), 3.36 (td, *J* = 1.1, 0.5 Hz, 2H), 3.05-2.99 (m, 4H), 2.91-2.87 (m, 2H), 2.33-2.31 (m, 2H), 1.46-1.45 (m, 2H), 1.34 (s, 9H). **LCMS**: t_R = 6.34 min, m/z = 575.0 $[M+H]^+$.

4-(4-((4-(4-(5-Aminopentanoyl)piperazin-1-yl)phenyl)amino)pyrimidin-2-yl)-*N*-(cyanomethyl)benzamide (S6)

To a magnetically stirred solution of compound **S5** (190 mg, 0.33 mmol) in DMF (6 mL, anhydrous) at room temperature under N_2 was added triethylamine (264 μL, 1.99 mmol) and the mixture was sonicated for 5 min. Then EDCI (76 mg, 0.40 mmol) and HOBt (54 mg, 0.40 mmol) were added and the mixture was stirred for 5 min under N_2. Then aminoacetonitrile hydrochloride (61 mg, 0.66 mmol) was added and the reaction was stirred at room temperature under N_2 for 12 h. The reaction mixture was concentrated and the crude material was purified by Flash chromatography to afford the coupled product (155 mg, 76%) as a yellow solid. This material was immediately dissolved in dioxane (0.5 mL) then HCl was added (1 mL of a 4 M solution in dioxane) and the reaction mixture stirred for 2 h at room temperature. Then the precipitate was collected by filtration and washed with dioxane before being dissolved in MeOH, and quenched with NH_3 (4 M solution in MeOH) then concentrated. The crude material was purified by Flash chromatography to afford the *title amine* (**S6**) as a yellow solid (51 mg, 40%). **^{1}H-NMR** (600 MHz,

CD_3OD): δ 8.37 (d, *J* = 5.2 Hz, 1H), 8.16 (d, *J* = 8.3 Hz, 2H), 7.91 (d, *J* = 8.3 Hz, 2H), 7.57 (d, *J* = 8.8 Hz, 2H), 7.20 (d, *J* = 5.2 Hz, 1H), 6.93 (d, *J* = 8.9 Hz, 2H), 4.34 (s, 2H), 3.69 (t, *J* = 5.1 Hz, 2H), 3.63 (t, *J* = 5.0 Hz, 2H), 3.30-3.29 (m, 2H), 3.07 (t, *J* = 5.0 Hz, 2H), 3.03 (t, *J* = 5.1 Hz, 2H), 2.67 (t, *J* = 7.2 Hz, 2H), 2.41 (t, *J* = 7.4 Hz, 2H), 1.62 (dt, *J* = 15.3, 7.6 Hz, 2H), 1.51 (td, *J* = 11.3, 6.1 Hz, 2H). **LCMS**: t_R = 4.18 min, m/z = 513.0 $[M+H]^+$.

Covalent coupling of CYT-387 kinase affinity reagent to NHS-sepharose

The modified CYT-387 compound was immobilized onto NHS-activated sepharose 4 Fast Flow beads (GE Healthcare) as previously described[46]. Briefly, 1 mL slurry of NHS-sepharose beads was washed twice with 5 mL DMSO, centrifuging at 80 *x* g for 3 min to pellet the matrix in between washes. One packed matrix volume (500 µL) was resuspended with DMSO as a 50% slurry. CYT-387 (2 µM final) was added to the 1 mL slurry of NHS-beads followed by 20 µL of triethylamine and mixed by inversion. The reaction slurry was incubated overnight at room temperature on an end-over-end rotator protected from light. The following day, 25 µL ethanolamine was added to the reaction and again left to incubate overnight at room temperature on an end-over-end rotator protected from light. The CYT-387-coupled NHS-sepharose beads were washed twice with 5 mL DMSO and the matrix was resuspended in ethanol and stored at 4 °C protected from light.

Kinase enrichment from cell lysates

CYT-387-bound resin was washed twice with KALB lysis buffer prior to kinase enrichment. Six individual kinase enrichments were performed (three per $Cish^{-/-}$ or $Cish^{+/+}$) with 160 µL of 50% Cyt387-bound resin incubated with 2 mL (~10 mg) of protein lysate. Incubations were performed for 3 h on a rotating wheel protected from light at 4 °C. Following incubation, protein-bound Cyt387 resins were washed 3 times with KALB buffer and eluted with 3 consecutive rounds of incubation with 0.5% SDS/5 mM DTT (200 µL, 100 µL, 100 µL) for 3 min at 60 °C.

Trypsin digestion

Eluates of resin-captured proteins along with equal amounts of whole cell lysate (~400 µg) derived from each biological replicate were prepared for mass spectrometry analysis using the FASP protein digestion kit (Protein Discovery, Knoxville, TN) as previously described[47], with the following modifications. Proteins were reduced with Tris-(2-carboxyethyl)phosphine (TCEP) (5 mM final concentration), digested with 4 µg of sequence-grade modified Trypsin Gold (Promega) in 50 mM NH_4HCO_3 and incubated overnight at 37 °C. Peptides were then eluted with 50 mM NH_4HCO_3 in two 40 µL sequential washes and acidified in 1% formic acid (final concentration).

Mass spectrometry and data analysis

Acidified peptide mixtures were analyzed by nanoflow reversed-phase liquid chromatography tandem mass spectrometry (LC-MS/MS) on a nanoAcquity system (Waters, Milford, MA, USA), coupled to a Q-Exactive mass spectrometer equipped with a nanoelectrospray ion source for automated MS/MS (Thermo Fisher Scientific, Bremen, Germany). Peptide mixtures were loaded on a 20 mm trap column with 180 µm inner diameter (nanoAcquity UPLC 2G-V/MTrap 5 mm Symmetry C_{18}) in buffer A (0.1% formic acid, 3% acetonitrile, Milli-Q water), and separated by reverse-phase chromatography using a 150 mm column with 75 µm inner diameter (nanoAcquity UPLC 1.7 µm BEH130 C_{18}) on a 60 min linear gradient set at a constant flow rate of 400 nL/min from 3-55% buffer B (0.1% formic acid, 80% acetonitrile, Milli-Q water). The Q-Exactive was operated in a data-dependent mode, switching automatically between one full-scan and subsequent MS/MS scans of the ten most abundant peaks. The instrument was controlled using Exactive series version 2.1 build 1502 and Xcalibur 3.0. Full-scans (m/z 350–1,850) were acquired with a resolution of 70,000 at 200 m/z. The 10 most intense ions were sequentially isolated with a target value of 10000 ions and an isolation width of 2 m/z and fragmented using HCD with normalized collision energy of 19.5 and stepped collision energy of 15%. Maximum ion accumulation times were set to 50 ms for full MS scan and 200 ms for MS/MS. Underfill ratio was set to 5% and dynamic exclusion was enabled and set to 90 sec.

Raw files consisting of high-resolution MS/MS spectra were processed with MaxQuant (version 1.5.0.25) for feature detection and protein identification using the Andromeda search engine[48]. Extracted peak lists were searched against the UniProtKB/Swiss-Prot *Mus musculus* database (LudwigNR) and a separate reverse decoy database to empirically assess the false discovery rate (FDR) using a strict trypsin specificity allowing up to 3 missed cleavages. The minimum required peptide length was set to 7 amino acids. Modifications: Carbamidomethylation of Cys was set as a fixed modification, while N-acetylation of proteins, oxidation of Met, the addition of pyroglutamate (at N-termini Glu and Gln), phosphorylation (Ser, Thr and Tyr), deamidation (Asn, Gln and Arg), were set as variable modifications. The mass tolerance for precursor ions and fragment ions were 20 ppm and 0.5 Da, respectively. The "match between runs" option in MaxQuant was used to transfer identifications made between runs on the basis of matching precursors with high mass accuracy[49]. PSM and protein identifications were filtered using a target-decoy approach at a false discovery rate (FDR) of 1%. Protein identification was based on a minimum of two unique peptides.

Quantitative proteomics pipeline

Further analysis was performed using a custom pipeline developed in Pipeline Pilot (Biovia) and R, which utilizes the MaxQuant output files allPeptides.txt, peptides.txt and evidence.txt. A feature was defined as the combination of peptide sequence, charge and modification. Features not found in at least half the number of replicates in each group were removed. Proteins identified from hits to the reverse database and proteins with only one unique peptide were also removed. To correct for injection volume variability, feature intensities were normalized by converting to base 2 logarithms and then multiplying each value by the ratio of maximum median intensity of all replicates over median replicate intensity. Features assigned to the same protein differ in the range of intensity due to their chemico-physical properties and charge state. To further correct for these differences, each intensity value was multiplied by the ratio of the maximum of the median intensities of all features for a protein over the median intensity of the feature. Missing values where imputed using a random normal distribution of values with the mean set at mean of the real distribution of values minus 1.8 standard deviations, and a standard deviation of 0.5 times the standard deviation of the distribution of the measured intensities[50]. The probability of differential expression between groups was calculated using the Wilcoxon Rank Sum test excluding any non-unique sequences and any features with modifications other than oxidation and carbamidomethylation. The output of the R function wilcox.test included *p*-value, confidence interval and ratio estimate. Probability values were corrected for multiple testing using Benjamini–Hochberg method. Cut-off lines with the function $y= -\log_{10}(0.05)+c/(x-x_0)$[51] were introduced to identify significantly enriched proteins. c was set to 0.2 while x_0 was set to 1 representing proteins with a with a 2-fold (log2 protein ratios of 1 or more) or 4-fold (log2 protein ratio of 2) change in protein expression, respectively. The log2-transformed summed peptide intensities (non-imputed) were visualized in a heat map generated in one-matrix CIMminer, a program developed by the Genomics and Bioinformatics Group (Laboratory of Molecular Pharmacology, Center for Cancer Research, National Cancer Institute).

Preparation of GST-CIS protein for peptide screening

Human *Cish* (residues 66-258) was cloned into the vector pGTVL2. Human Elongin C (residues 17–112) and full length Elongin B were cloned into the vector pACYCDUET as previously described[52]. Both plasmids were transformed into BL21(DE3) for co-expression of the CIS/Elongin C/Elongin B ternary complex (CIS-SH2-BC). Cultures in Luria broth media were induced with 0.4 mM isopropyl β-D-1-thiogalactopyranoside (IPTG) overnight at 18°C and the cells harvested by centrifugation. Pellets were resuspended in 50 mM HEPES pH 7.5, 500 mM NaCl, 5 mM imidazole, 5% glycerol and the cells lysed by sonication. DNA was precipitated by addition of 0.15% polyethyleneimine pH 8 and the insoluble material excluded by centrifugation at 21,000 rpm. The GST-tagged CIS protein complex was purified on a glutathione sepharose column and

eluted with 20 mM reduced glutathione in a buffer comprising 50 mM HEPES, 300 mM NaCl, 0.5 mM TCEP. The purified protein was concentrated to 0.75 mg/ml and stored at -80°C.

Peptide array synthesis and screening

The peptide arrays were synthesized on functionalized nitrocellulose membranes using an Invatis spot array synthesizer as described[53]. For array probing, the membrane-bound peptides were blocked at room temperature for 5 h in 5% skim milk of Tris-buffered saline/0.05% Tween-20 (TBS-T), pH 7.2. After washing with TBS-T, 0.8 ng/ml of GST-CIS-SH2-BC complex was added in blocking buffer and incubated at 4 °C overnight. At the same time, 4 ng/ml of GST protein was added to a separate peptide array as a negative control under the same experimental conditions. The peptide array membranes were washed with TBS-T 3x, and a peroxidase-labeled anti-GST antibody (Bio-Rad) added at room temperature for 1 h, prior to detection with a chemiluminescence substrate (Bio-Rad Clarity Western ECL Substrate), which was visualized using a Molecular Imager (ChemiDoc XRS; Biorad).

Isothermal titration calorimetry (ITC)

Isothermal calorimetric titrations were performed with a Microcal ITC200 (GE Healthcare). Phosphopeptides were obtained from Genscript. An optimized GST-CIS protein construct was prepared in which the internal PEST region (Δ174-202) was deleted. The resulting ternary GST-CIS-SH2-SB complexes were dialyzed against buffer (20 mM Tris pH 8.0, 100 mM NaCl, 2 mM 2-mercaptoethanol). Experiments were performed at 298 K unless stated otherwise. Typically, 12x 3.15 μl injections of 300 μM phosphopeptides were titrated into a 30 μM solution of the GST-CIS-SH2-SB ternary complex. The heat of dilution of GST-CIS-SH2-BC was subtracted from the raw data of the binding experiment. Data were analyzed using the evaluation software, Microcal Origin version 5.0. The binding curve fitted a single-site binding mode and all K_D values were determined from duplicate experiments.

E3 ligase assay

CIS-mediated ubiquitination of JAK1 was performed essentially as described previously[54]. The CIS E3 ligase complex (CIS-SH2-BC together with Cullin5 and Rbx2; 2.5 μM) was incubated with ubiquitin (50 μM), human E1 (100 nM), purified recombinant E2 (UbcH5c, 2.5 μM) and full-length JAK1 in the presence of 2.5 mM Mg/ATP at 37^{o}C for varying times. FLAG-tagged JAK1 was generated by expression in 293T cells and recovered using anti-FLAG immunoprecipitation and elution with free FLAG peptide. JAK1 ubiquitination was visualized by immunoblotting with anti-phosphorylated JAK1 following separation on 4-20% Tris/Glycine gels.

Kinase Assay

Kinase inhibition assays were performed essentially as described[55]. Briefly, 130 μM STAT5b peptide (RRAKAADGYVKPQIKQVV) was incubated with 5 nM $JAK1_{JH1}$ at 25°C for 30–60 min in 20 mM Tris pH 8.0, 100 mM NaCl, 5 mM 2-mercaptoethanol, 0.2 mg/ml bovine serum albumin, 2 mM $MgCl_2$, 100 μM ATP and 1 mCi γ-[32P]ATP. Recombinant CIS-SH2-BC was present at concentrations ranging from 0-30 μM. After incubation, the reaction was spotted onto P81 phosphocellulose paper and quenched in 5% H_3PO_4. The paper was washed (4 x 200 ml, 15 min) with 5% H_3PO_4 and exposed to a phosphorimager plate (Fuji). Quantitation was performed using Fuji software and IC_{50} curves calculated using Graphpad Prism.

Tumor cell lines

The C57BL/6 murine lymphoma cell line RMA is a T cell lymphoma derived from the Rauscher murine leukemia virus-induced RBL-5 cell line. The cell lines RMA-mCherry and $m157^+$RMA-GFP were generated by transduction with a retroviral vector (murine stem cell vector) encoding mCherry or GFP, respectively. B16F10 melanoma, E0771-mCherry+ and E0771.LMB-mCherry+ breast, LWT1 melanoma, and RM-1 prostate carcinoma cell lines, were maintained as previously described [56-62].

Experimental tumor metastasis

Groups of 6-14 mice per experiment were used for experimental tumor metastases. These group sizes were used to ensure adequate power to detect biological differences. No mice were excluded based on pre-established criteria in this study and no active randomization was applied to experimental groups. The investigators were not blinded to the group allocation during the experiment and/or when assessing the outcome. All tumor experiments were performed once unless specifically indicated. Single-cell suspensions of B16F10 melanoma, RM-1 prostate carcinoma, or LWT1 melanoma cells were injected i.v. into the tail vein of the indicated strains of mice (2.5-7.5x10^5 cells/mouse). Some mice additionally received either 100 μg anti-CD8β (53.5.8) as indicated to deplete $CD8^+$ T cells, 50 μg anti-asialoGM1 to deplete NK cells, or 250 μg anti-IFN-γ (H22) to neutralize IFN-γ as previously described[37,63]. Some groups of mice received on days 0, 3 and 6 relative to tumor inoculation (day 0) either: control Ig (500 μg i.p., cIg, 1-1) or combination anti-PD-1 (RMP1-14)/anti-CTLA-4 (UC10-4F10) (250 μg i.p. each). Lungs were harvested on day 14 and either fixed in Bouin's solution and B16F10 metastases counted[57] or analyzed for NK cell expansion by flow cytometry. For adoptive transfer models, *Mcl1*$^{f/f}$*Ncr1-iCre* mice[12] were injected i.v. with 3 x 10^6 *in vitro* expanded *Cish*$^{+/+}$ or *Cish*$^{-/-}$ NK cells or PBS. Mice were then injected 8 h

later with 1 x 10^5 B16F10 melanoma cells. Mice were subsequently treated on day 1 with 1.5 x 10^6 *in vitro* expanded *Cish*$^{+/+}$ or *Cish*$^{-/-}$ NK cells or PBS delivered i.v. Mice were sacrificed on day 18 following tumor injection and lung perfusion performed. Lungs were then harvested and metastases counted.

Orthotopic E0771.LMB and spontaneous E0771 metastasis

To generate primary tumors, 1×10^5 E0771.LMB mCherry+ tumor cells were implanted into the fourth inguinal mammary gland [in 20 µl of PBS] of 8- to 10-week-old female *Cish*$^{-/-}$ or *Cish*$^{+/+}$ mice. Primary tumor volume was measured three times per week using electronic callipers. The greatest longitudinal diameter (length) and the greatest transverse diameter (width) were measured. Tumor volumes were estimated by the modified ellipsoidal formula: volume=1/2(length×width^2). For spontaneous metastasis experiments, primary tumors were surgically resected at a size of 400–600 mm^3. Lungs were harvested 14 days later and metastatic burden quantified by imaging *ex vivo* using an IVIS Lumina XR-III (Caliper Life Sciences) or by duplex Q-PCR for expression of mCherry relative to vimentin, as described previously[61].

ONLINE METHODS REFERENCES

39 Croker, B. A. *et al.* SOCS3 negatively regulates IL-6 signaling in vivo. *Nature immunology* **4**, 540-545, doi:10.1038/ni931 (2003).

40 Alexander, W. S. *et al.* SOCS1 is a critical inhibitor of interferon gamma signaling and prevents the potentially fatal neonatal actions of this cytokine. *Cell* **98**, 597-608 (1999).

41 Narni-Mancinelli, E. *et al.* Fate mapping analysis of lymphoid cells expressing the NKp46 cell surface receptor. *Proc Natl Acad Sci U S A* **108**, 18324-18329, doi:10.1073/pnas.1112064108 (2011).

42 Boyman, O. *et al.* Selectively expanding subsets of T cells in mice by injection of interleukin-2/antibody complexes: implications for transplantation tolerance. *Transplantation proceedings* **44**, 1032-1034, doi:10.1016/j.transproceed.2012.01.093 (2012).

43 Kolesnik, T. B. & Nicholson, S. E. Analysis of Suppressor of Cytokine Signalling (SOCS) gene expression by real-time quantitative PCR. *Methods in molecular biology* **967**, 235-248, doi:10.1007/978-1-62703-242-1_17 (2013).

44 Nicholson, S. E., Novak, U., Ziegler, S. F. & Layton, J. E. Distinct regions of the granulocyte colony-stimulating factor receptor are required for tyrosine phosphorylation of the signaling molecules JAK2, Stat3, and p42, p44MAPK. *Blood* **86**, 3698-3704 (1995).

45 Linossi, E. M. *et al.* Suppressor of Cytokine Signaling (SOCS) 5 utilises distinct domains for regulation of JAK1 and interaction with the adaptor protein Shc-1. *PloS one* **8**, e70536, doi:10.1371/journal.pone.0070536 (2013).

46 Schirle, M. *et al.* in *Kinase Inhibitors* Vol. 795 *Methods in Molecular Biology* (ed Bernhard Kuster) Ch. 11, 161-177 (Humana Press, 2012).

47 Wisniewski, J. R., Zougman, A., Nagaraj, N. & Mann, M. Universal sample preparation method for proteome analysis. *Nature methods* **6**, 359-362, doi:10.1038/nmeth.1322 (2009).

48 Cox, J. *et al.* Andromeda: a peptide search engine integrated into the MaxQuant environment. *Journal of proteome research* **10**, 1794-1805, doi:10.1021/pr101065j (2011).
49 Cox, J. & Mann, M. MaxQuant enables high peptide identification rates, individualized p.p.b.-range mass accuracies and proteome-wide protein quantification. *Nature biotechnology* **26**, 1367-1372, doi:10.1038/nbt.1511 (2008).
50 Cox, J. *et al.* Accurate proteome-wide label-free quantification by delayed normalization and maximal peptide ratio extraction, termed MaxLFQ. *Molecular & cellular proteomics : MCP* **13**, 2513-2526, doi:10.1074/mcp.M113.031591 (2014).
51 Keilhauer, E. C., Hein, M. Y. & Mann, M. Accurate protein complex retrieval by affinity enrichment mass spectrometry (AE-MS) rather than affinity purification mass spectrometry (AP-MS). *Molecular & cellular proteomics : MCP* **14**, 120-135, doi:10.1074/mcp.M114.041012 (2015).
52 Bullock, A. N., Debreczeni, J. E., Edwards, A. M., Sundstrom, M. & Knapp, S. Crystal structure of the SOCS2-elongin C-elongin B complex defines a prototypical SOCS box ubiquitin ligase. *Proc Natl Acad Sci U S A* **103**, 7637-7642 (2006).
53 Li, S. S. & Wu, C. Using peptide array to identify binding motifs and interaction networks for modular domains. *Methods in molecular biology* **570**, 67-76, doi:10.1007/978-1-60327-394-7_3 (2009).
54 Babon, J. J. & Murphy, J. M. In vitro JAK kinase activity and inhibition assays. *Methods in molecular biology* **967**, 39-55, doi:10.1007/978-1-62703-242-1_3 (2013).
55 Babon, J. J. *et al.* Suppression of cytokine signaling by SOCS3: characterization of the mode of inhibition and the basis of its specificity. *Immunity* **36**, 239-250 (2012).
56 Ferrari de Andrade, L. *et al.* Natural killer cells are essential for the ability of BRAF inhibitors to control BRAFV600E-mutant metastatic melanoma. *Cancer research* **74**, 7298-7308, doi:10.1158/0008-5472.CAN-14-1339 (2014).
57 Gilfillan, S. *et al.* DNAM-1 promotes activation of cytotoxic lymphocytes by nonprofessional antigen-presenting cells and tumors. *The Journal of experimental medicine* **205**, 2965-2973, doi:10.1084/jem.20081752 (2008).
58 Stagg, J. *et al.* CD73-deficient mice have increased antitumor immunity and are resistant to experimental metastasis. *Cancer research* **71**, 2892-2900, doi:10.1158/0008-5472.CAN-10-4246 (2011).
59 Stagg, J. *et al.* Anti-ErbB-2 mAb therapy requires type I and II interferons and synergizes with anti-PD-1 or anti-CD137 mAb therapy. *Proc Natl Acad Sci U S A* **108**, 7142-7147, doi:10.1073/pnas.1016569108 (2011).
60 Swann, J. B. *et al.* Type I IFN contributes to NK cell homeostasis, activation, and antitumor function. *Journal of immunology* **178**, 7540-7549 (2007).
61 Rautela, J. *et al.* Loss of Host Type-I IFN Signaling Accelerates Metastasis and Impairs NK-cell Antitumor Function in Multiple Models of Breast Cancer. *Cancer immunology research* **3**, 1207-1217, doi:10.1158/2326-6066.CIR-15-0065 (2015).
62 Johnstone, C. N. *et al.* Functional and molecular characterisation of EO771.LMB tumours, a new C57BL/6-mouse-derived model of spontaneously metastatic mammary cancer. *Disease models & mechanisms* **8**, 237-251, doi:10.1242/dmm.017830 (2015).
63 Allard, B., Pommey, S., Smyth, M. J. & Stagg, J. Targeting CD73 enhances the antitumor activity of anti-PD-1 and anti-CTLA-4 mAbs. *Clinical cancer research : an official journal of the American Association for Cancer Research* **19**, 5626-5635, doi:10.1158/1078-0432.CCR-13-0545 (2013).

[i] CANCER THERAPEUTICS CRC PTY LIMITED, Patent: WO2014/26242 A1, **2014**

[ii] CYTOPIA RESEARCH PTY LTD Patent: WO2008/109943 A1, **2008**

Figure 1

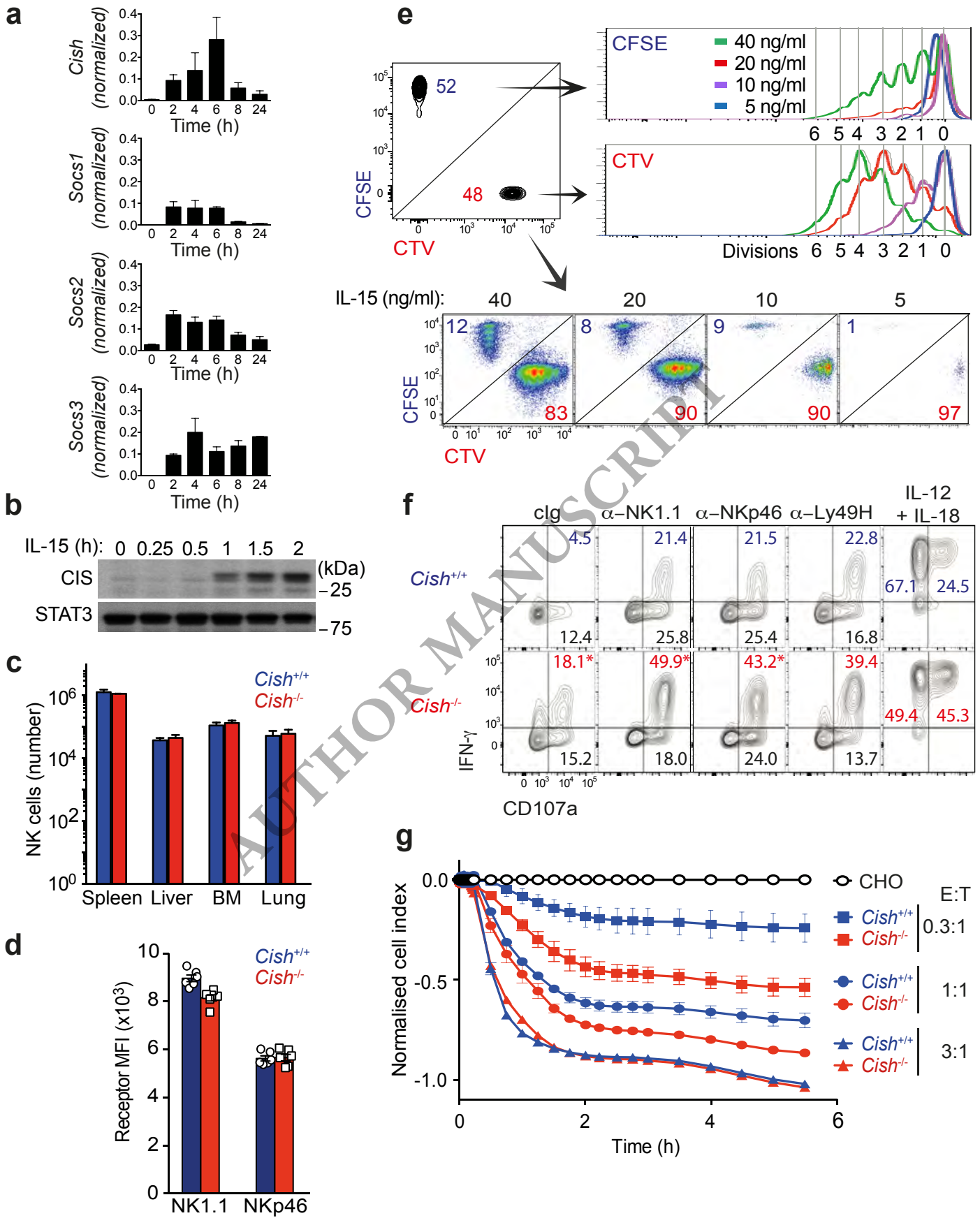

Figure 2

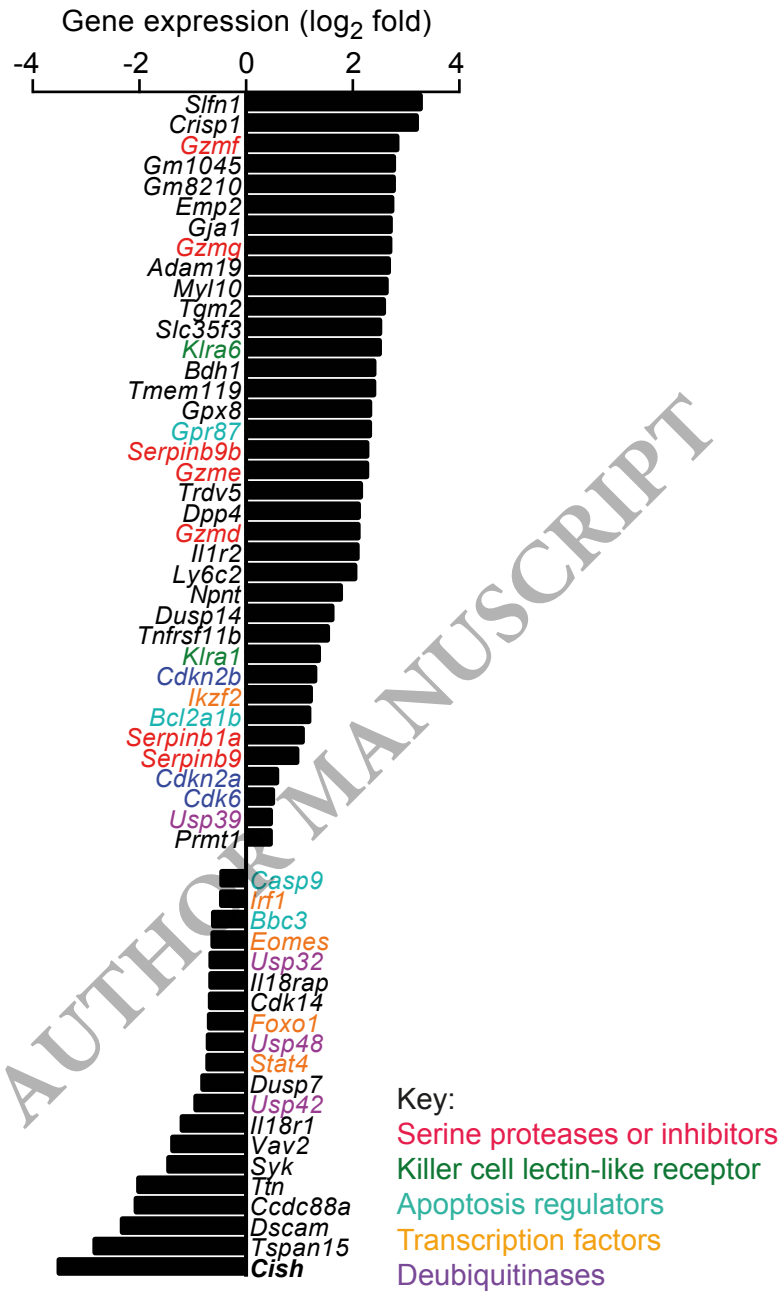

Figure 3

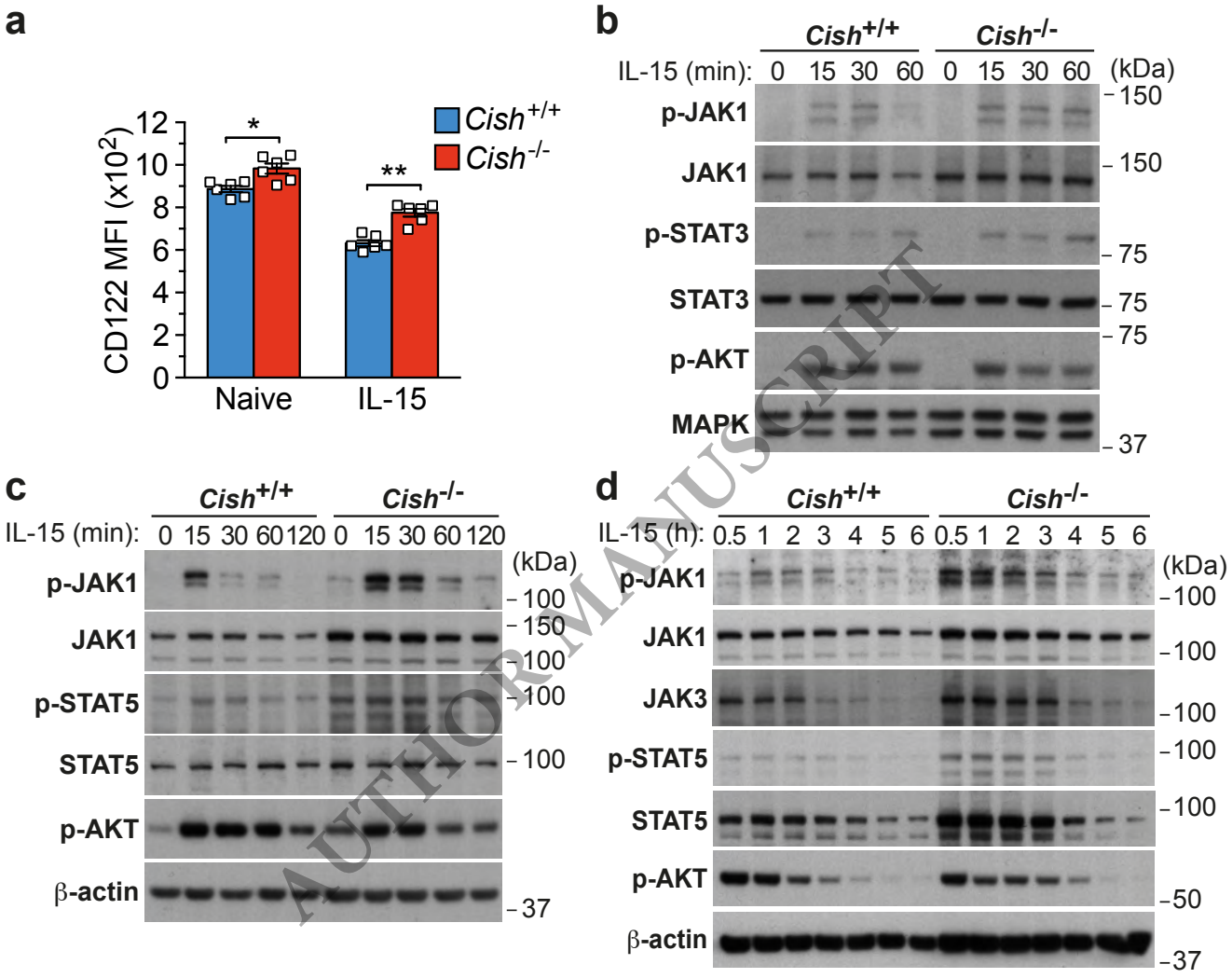

Figure 4

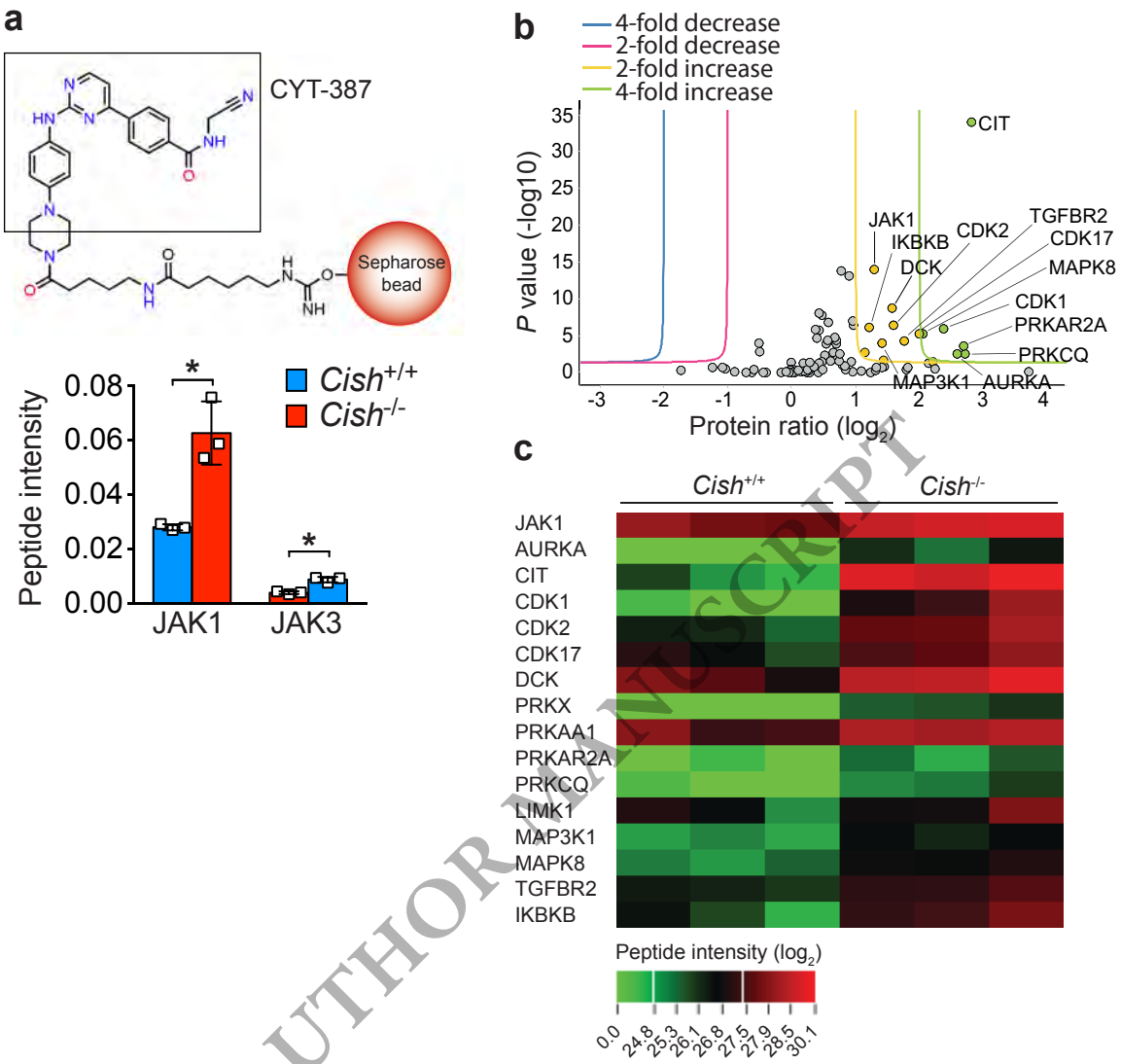

Figure 5

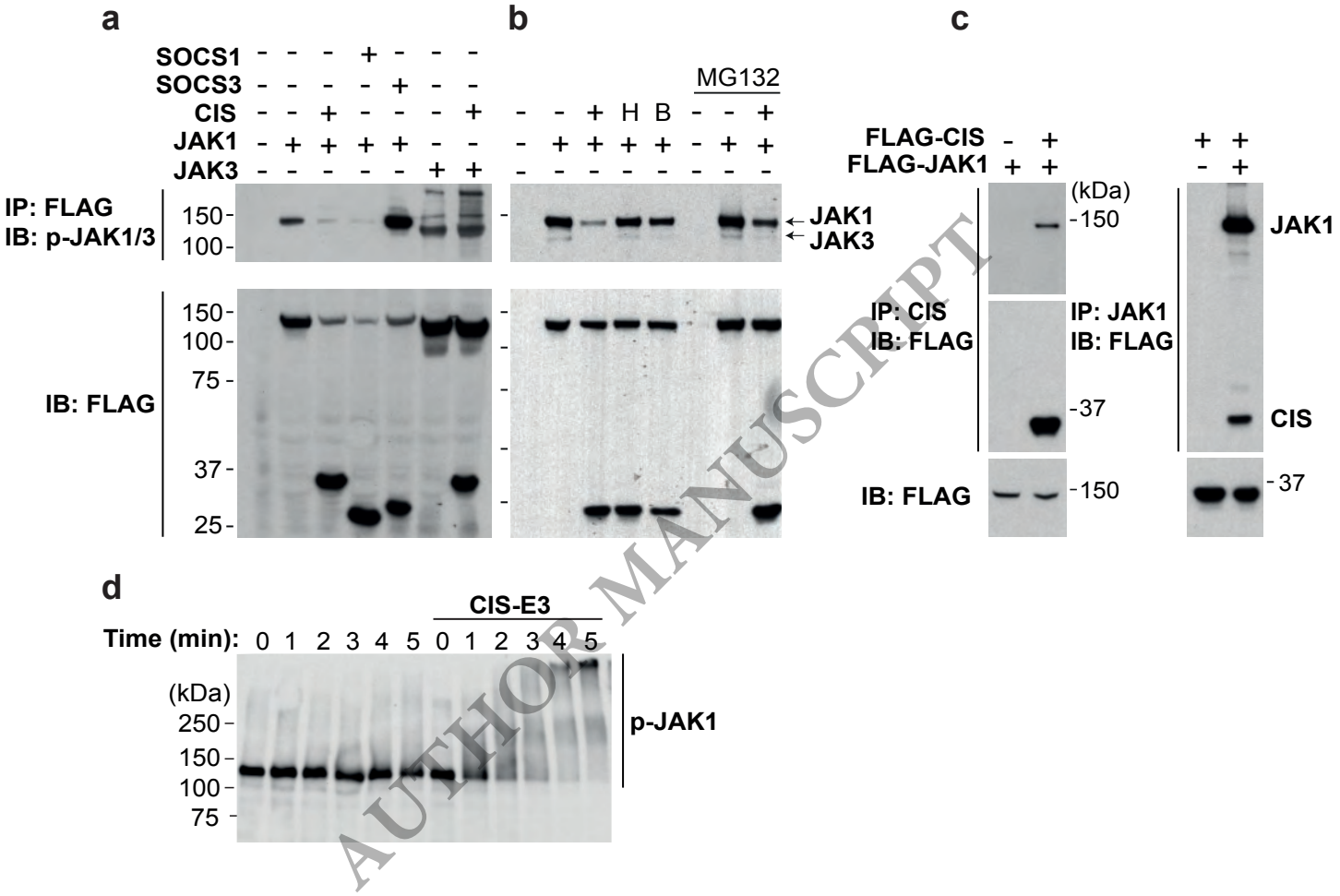

Figure 6

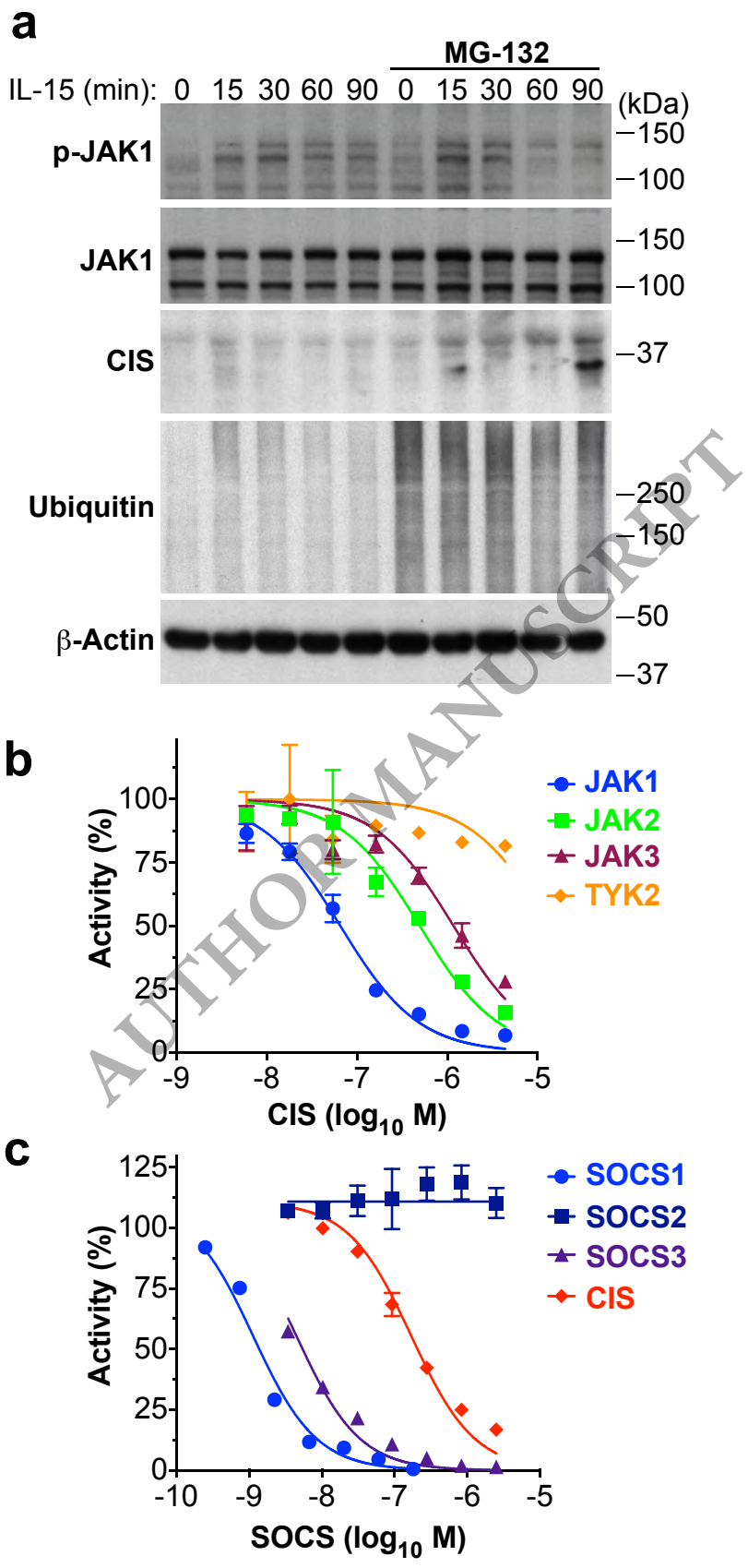

Figure 7

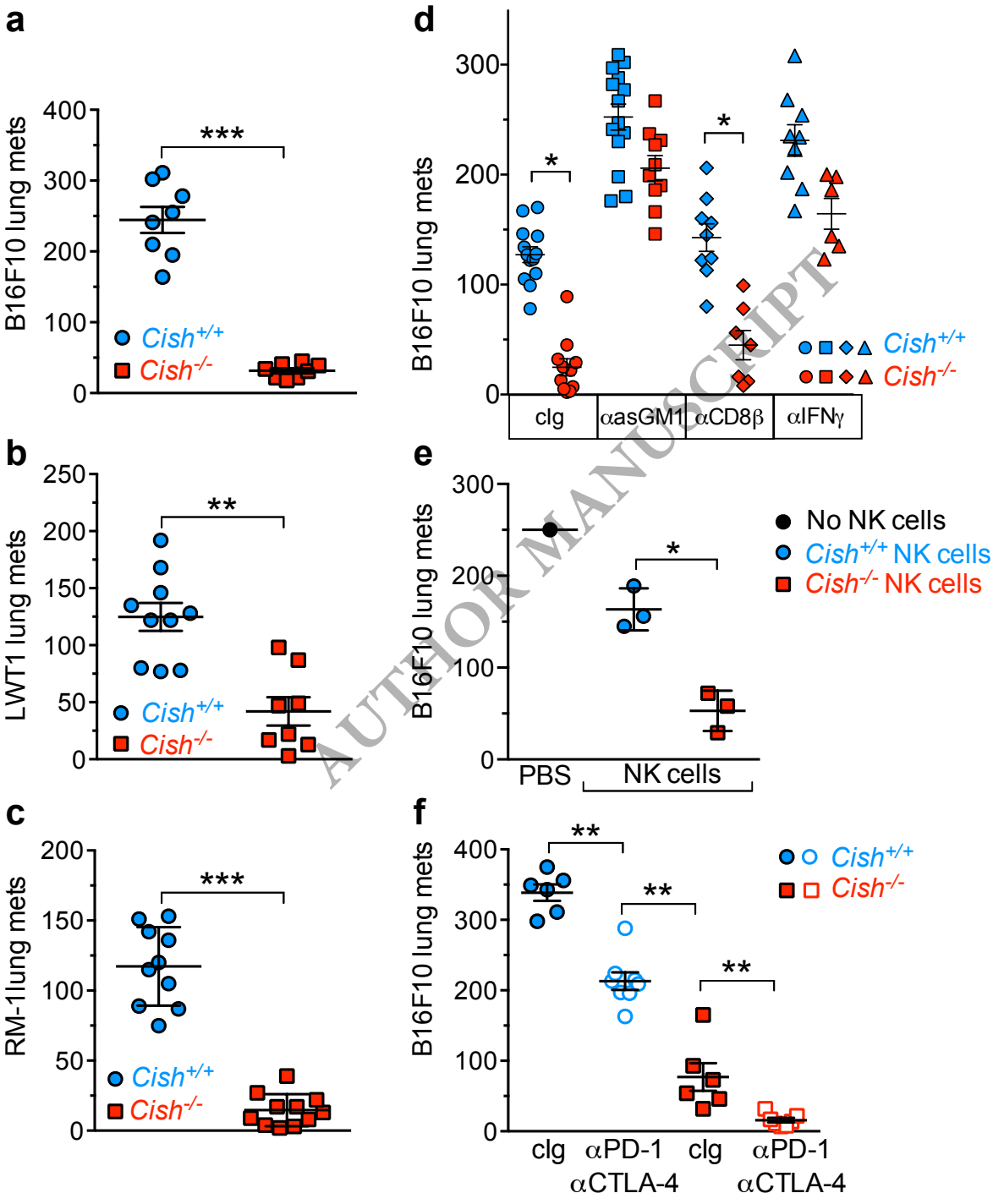

Figure 8